Shallow, Intermediate, and Deep Overturning Components of the Global Heat Budget

LYNNE D. TALLEY

Scripps Institution of Oceanography, University of California, San Diego, La Jolla, California

(Manuscript received 24 October 2001, in final form 9 September 2002)

ABSTRACT

The ocean's overturning circulation and associated heat transport are divided into contributions based on water mass ventilation from 1) shallow overturning within the wind-driven subtropical gyres to the base of the thermocline, 2) overturning into the intermediate depth layer (500–2000 m) in the North Atlantic and North Pacific, and 3) overturning into the deep layers in the North Atlantic (Nordic Seas overflows) and around Antarctica. The contribution to South Pacific and Indian heat transport from the Indonesian Throughflow is separated from that of the subtropical gyres and is small. A shallow overturning heat transport of 0.6 PW dominates the 0.8-PW total heat transport at 24°N in the North Pacific but carries only 0.1–0.4 PW of the 1.3-PW total in the North Atlantic at 24°N. Shallow overturning heat transports in the Southern Hemisphere are also poleward: −0.2 to −0.3 PW southward across 30°S in each of the Pacific and Indian Oceans but only −0.1 PW in the South Atlantic. Intermediate water formation of 2 and 7 Sv (1 Sv $\equiv 10^6$ m^3 s^{-1}) carries 0.1 and 0.4 PW in the North Pacific and Atlantic, respectively, while North Atlantic Deep Water formation of 19 Sv carries 0.6 PW. Because of the small temperature differences between Northern Hemisphere deep waters that feed the colder Antarctic Bottom Water (Lower Circumpolar Deep Water), the formation of 22 Sv of dense Antarctic waters is associated with a heat transport of only −0.14 PW across 30°S (all oceans combined). Upwelling of Circumpolar Deep Water north of 30°S in the Indian (14 Sv) and South Pacific (14 Sv) carries −0.2 PW in each ocean.

1. Introduction

In the heat balance of the earth, the oceans have been thought to carry approximately one-third to one-half of the excess heat from the tropical regions toward higher latitudes (e.g., Hsiung 1985; Keith 1995). New satellite observations of the top-of-the-atmosphere radiation budget suggest higher total heat transports than previous analyses and, depending on the analysis product used for the atmosphere, have reduced the relative fraction of ocean heat transport in the total (Keith 1995; Trenberth et al. 2001). Estimates of ocean heat transports, on the other hand, have been converging. The results presented here with a different basic circulation analysis (Reid 1994, 1997) are consistent with those published over the last 20 years. Trenberth and Caron (2001) show a maximum total poleward heat transport of 5 PW at midlatitudes, of which the ocean carries about 2 PW, as is also seen here.

In the ocean, poleward heat transport is associated with transformation of warm waters into colder waters, through mostly well-identified water mass formation and transformation processes. Heat budgets for the ocean are computed in terms of total heat carried into a closed region and hence are equal to the total heat flux across the ocean–atmosphere interface (assuming small heat flux from the ocean floor). Emphasis is usually placed on the total heat transport carried at all depths/temperatures into or out of the closed region. However, calculation of heat transports in terms of mass-balanced water mass formation processes can help reveal and quantify the dominant transformation processes. Adequate simulation of these processes in coupled models should not only produce realistic heat budgets but should also be a prerequisite for the usefulness of the models for simulating climate.

The primary goal here is to estimate the heat transport carried by the shallow, subducting part of the subtropical gyres separately from that associated with deeper meridional overturn, and then to estimate the relative importance of intermediate, deep, and bottom water overturn within the latter. To this end, mass-balanced portions of the circulation are chosen based on layer outcrops at the sea surface in winter, identification of western boundary currents and other discrete parts of the circulation, and identifiable intermediate and deep water masses. This procedure differs from most previous decompositions of heat transport associated with different ocean processes through its more water mass–based identification of the components and its strict use of isopycnal layers.

Many direct heat transport estimates for the ocean

Corresponding author address: Lynne D. Talley, Scripps Institution of Oceanography, University of California, San Diego, 9500 Gilman Drive, La Jolla, CA 92093-0230.
E-mail: ltalley@ucsd.edu

have been published, using velocity and temperature observations across all of the midlatitude subtropical gyres and at a number of other locations, using both pre–World Ocean Circulation Experiment (WOCE) and WOCE observations. Bryden and Imawaki (2001) review many produced before 2000. Notable recent contributions for comparison here are the Southern Ocean analyses of Sloyan and Rintoul (2001a,b) and Wijffels et al. (2001). General patterns of ocean heat transport include northward heat transport in the Northern Hemisphere oceans, southward transport in the South Pacific and Indian Oceans (both including the Indonesian Throughflow as part of the closed sections), and northward transport in the South Atlantic Ocean, the last resulting from the overturning circulation associated with North Atlantic Deep Water formation. Meridional heat transport in the North Pacific is dominated by the shallow wind-driven circulation (Bryden et al. 1991) while North Atlantic transport is more dominated by formation of North Atlantic Deep Water (e.g., Hall and Bryden 1982; Roemmich and Wunsch 1985). The relative contribution of Northern Hemisphere intermediate water formation to heat transport has not really been addressed, nor have the Southern Hemisphere heat transports been separated into shallow, deep, and Indonesian Throughflow (ITF) overturning loops, except nonquantitatively (Talley 1999).

Direct estimates of lateral ocean heat transport, based on in situ temperature and horizontal velocity, are meaningful only for mass-balanced components since they then provide heat flux divergences and convergences that can be compared with ocean–atmosphere heat fluxes. Zonal hydrographic sections only are used here. Atlantic and Pacific sections must be closed with the transport through the Bering Strait, while South Pacific and Indian sections are also closed with transport through the Indonesian archipelago. Reid's (1994, 1997) geostrophic velocity analyses for the Atlantic and Pacific Oceans are used here, modified to include Ekman transport. Indian Ocean volume and heat transports were provided by P. Robbins (1999, personal communication) using a small update to Robbins and Toole (1997) incorporating lowered acoustic Doppler current profiler (LADCP) constraints on the Agulhas transports from Beal and Bryden (1999). Reid (1994) and Reid (1997) are referred to henceforth as ''RAtl'' and ''RPac'' and Robbins and Toole (1997) as ''RTInd.''

Before examining heat transports in terms of mass-balanced subportions of the circulation, total heat transports are shown for comparison with previous heat transport estimates. As total heat transports based on the RAtl/RPac circulation have not been calculated before, all of Reid's zonal sections are included and reproduce what is already widely known about meridional ocean heat transports. The volume and heat transports at subtropical latitudes are then separated into various water mass and hence process-based components, with mass balanced for each: 1) The shallowest component is associated with the wind-driven subtropical gyres in which warm waters are advected poleward by western boundary currents, cooled, and returned southward in the interior in the subducted layers (in and above the thermocline). 2) The intermediate and deep components are associated either with poleward transport of warm waters that are transformed at subpolar and higher latitudes to higher densities and then return, or with poleward transport of deep waters that are warmed and upwell. 3) Heat transport associated with the Indonesian Throughflow, fed by northward flow through the South Pacific and leading to southward flow through the Indian Ocean, is calculated. 4) The small Bering Strait throughput, northward through the Pacific and southward through the Atlantic, also has an associated heat transport. Roemmich and Wunsch (1985) used this type of decomposition, based on maximum ventilation density, for the North Atlantic 24°N section. This decomposition differs from the barotropic, baroclinic, and horizontal heat flux decomposition summarized by Bryden and Imawaki (2001) and applied here for comparison (appendix A).

The datasets are described in section 2 and appendix C, the total heat transports in section 3, and the heat transport decomposition into shallow and intermediate/deep overturning cells in section 4. Appendices include the barotropic, baroclinic, and horizontal heat flux decomposition (appendix A); a comparison of heat transports using the National Centers for Environmental Prediction (NCEP) annual-averaged winds with those using the Hellerman and Rosenstein (1983) winds (appendix B); and data quality comments (appendix C).

2. Method and datasets

a. Heat and temperature transports

Direct estimates of lateral heat transport through a vertical cross-sectional area require velocity, temperature, and salinity observations. Volume, mass, heat, salinity, and freshwater transports are given by

$$V = \iint v \, dA \tag{1a}$$

$$M = \iint \rho v \, dA \tag{1b}$$

$$H = \iint \rho c_p \theta v \, dA \tag{1c}$$

$$S = \iint \rho s v \, dA \tag{1d}$$

$$F = M - S = \iint \rho v (1 - s) \, dA, \tag{1e}$$

where ρ, v, c_p, θ, and s are in situ density (kg m^{-3}), velocity normal to the area (m s^{-1}), specific heat of

seawater (J kg^{-1} $°C^{-1}$) using potential temperature and 0 dbar, potential temperature (°C), and salinity (kg kg^{-1}). When integrated over a vertical section, where $dA = dxdz$, and where the section (or section plus a strait flow) is closed, mass must be nearly conserved (with a small residual due to the external freshwater fluxes). Salt transport is then zero, mass and freshwater transport are balanced by precipitation–evaporation–runoff ($P - E + R$), and heat transport is balanced by air–sea heat flux in the area enclosed by the section or sections. The usual assumption for heat transport is that mass is conserved (Wijffels 2001) since the freshwater transport is no larger than 1 Sv (Sv $\equiv 1 \times 10^6$ m^3 s^{-1}) anywhere, which is smaller than the error in mass transport (section 2c). The freshwater balances from this dataset are being calculated and presented separately. Also, volume transports (1a) rather than mass transports are commonly used and are used here, again with small error compared with the true error in mass balance.

The term ''temperature transport,'' from Hall and Bryden (1982), refers to the quantity in the integral in (1c) for heat transport when mass is not conserved, and is useful for non-mass-balanced intermediate steps toward the total heat transport calculation (for which mass is balanced in the sense described above). To make the calculations easier to follow, the usual ''PW'' is the abbreviation for petawatt (1×10^{15} W) when referring to heat transport with balanced mass, while an ad hoc abbreviation ''PWT'' (also 1×10^{15} W) is introduced for temperature transport. Temperatures are in degrees Celsius.

All transports estimated here are quasi-meridional, based on geostrophic velocity and Ekman transports normal to quasi-zonal hydrographic sections (Fig. 1 and Table 1). Some sections are pieced from multiple cruises (RAtl, RPac, and appendix C). The decomposition in section 4 is focused on the subtropical sections at 24°N in the Northern Hemisphere and approximately 30°S in the Southern Hemisphere. The method for calculating the shallow overturning heat transport associated with the ventilated layer of the subtropical gyres and the heat transport associated with intermediate and deep water formation is given in section 4.

b. Data sources

Geostrophic reference velocities and total volume transports for every hydrographic station pair on the Atlantic and Pacific sections were provided by J. Reid (1998, personal communication). Reid's (RAtl and RPac) circulations are internally consistent, equivalent to those of ocean-basin-scale global inverse box models, with attention to initial reference velocity choices in every region, based on tracer patterns on isopycnals. Reid's geostrophic velocities balance mass, allowing for Bering Strait and Indonesian passage throughflows, within a small error for each closed section. Reid's circulations do not include Ekman transport. Thus it was necessary to add Ekman transport here and then to adjust the geostrophic circulations for overall mass balance, as described below.

P. Robbins, (1999, personal communication) provided isopycnal layer transports for the Indian Ocean hydrographic section at 32°S, slightly amended from the original analysis in RTInd through inclusion of direct velocity observations in the Agulhas (Beal and Bryden 1999). These transports are complete, including Ekman transport from Hellerman and Rosenstein (1983). Bryden and Beal's (2001) recent inverse solution for the same Indian Ocean section, incorporating Agulhas Current velocity observations, could also have been a useful basis for the calculation here, with somewhat smaller deep overturn transports than RTInd. Because both conserve silica, both analyses yield much smaller deep upwelling than the original Toole and Warren (1993) calculation. Sloyan and Rintoul (2001a) could have also been a useful starting point, with a larger deep overturn of 23 Sv, but with a smaller net heat transport.

To close the mass balance for heat transport, meridional transports across the Indian and South Pacific sections must be paired with the flow through the Indonesian archipelago (Indonesian Throughflow or ITF). Transports for all sections in the Pacific and Atlantic must be paired with the Bering Strait transport. Thus the ''heat transport'' across a given zonal section is actually the net heat loss or gain in the large regions defined by the zonal sections plus ITF and/or Bering Strait. Bering Strait carries 0.86 Sv northward out of the Pacific (Roach et al. 1995), with a temperature assigned here of 0°C and hence a (convenient) temperature transport of 0 PWT. Because the ITF is so warm and the associated heat transport is of the same magnitude as other components of the overturning circulation, a good estimate of its strength is necessary for heat and freshwater budgets (e.g., Talley 1984; Wijffels et al. 1992; Toole and Warren 1993; Macdonald 1993; Robbins and Toole 1997; Sloyan and Rintoul 2001a,b; Wijffels et al. 2001; Bryden and Beal 2001). The archipelago has been the subject of recent intensive observations (Gordon et al. 1999; Chong et al. 2000), yielding an ITF transport of 9.3 Sv $\pm$ 2.5 Sv (Gordon et al. 1999). An average temperature of 15°C has been observed for the ITF and is used here, with a temperature transport of 0.50 PWT (Vranes et al. 2002), noting that RTInd used 24°C and a higher temperature transport. The new, lower temperature transport reduces the impact of the ITF on the subtropical heat budgets calculated below.

RTInd assumed 8 Sv for the ITF, close to recent observations (Vranes et al. 2002). RPac assumed a net transport of 5 Sv northward in the South Pacific and about 2 Sv northward in the North Pacific, thus transports of 3 Sv for the Indonesian Throughflow and 2 Sv for the Bering Strait flow. This has been adjusted slightly in concept here for the South Pacific to 4 Sv for the Indonesian Throughflow and 1 Sv for the Bering Strait flow. For consistency with RTInd's 8 Sv and the recent

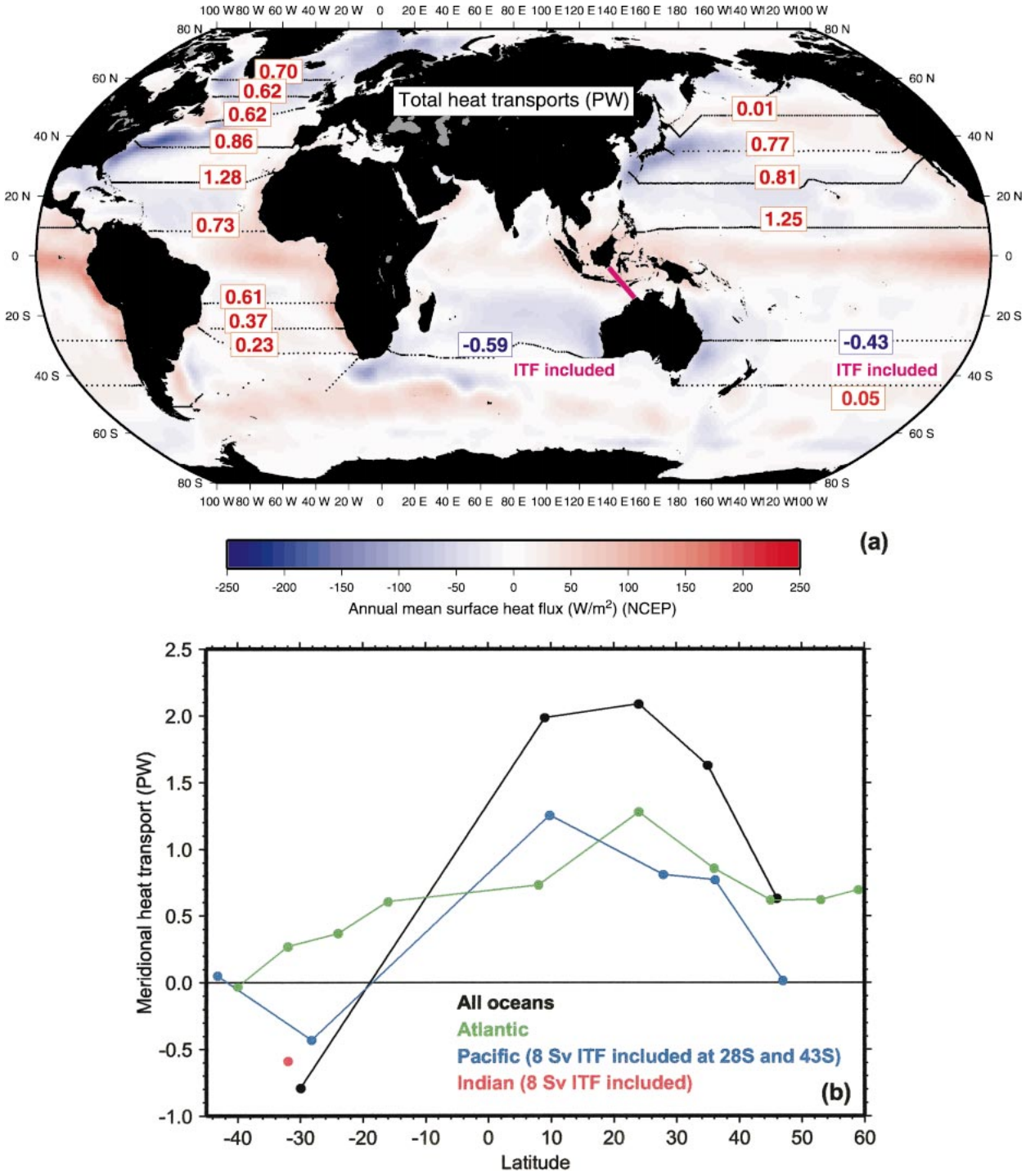

FIG. 1. (a) Total heat transport (PW) for each zonal section (Table 1). The Indian transport is from Robbins and Toole (1997) with a slight modification in procedure (P. Robbins 1999, personal communication; see text). Atlantic and Pacific transports are based on Reid (1994, 1997) geostrophic velocities adjusted for mass balance (within the residual throughflow transports for the Indonesian archipelago and Bering Strait), with Ekman transports from Hellerman and Rosenstein (1983) annual averaged winds. Heat transports use these adjusted geostrophic velocities and associated temperatures, and Levitus and Boyer (1994) near-surface temperatures for Ekman transport. The annotated Indian Ocean ''32°S'' and South Pacific ''28°S'' and ''43°S'' heat transports each include 8 Sv of Indonesian Throughflow to close the total mass balance. Thus the ''heat transports'' are heat flux convergences for each ocean north of the zonal sections. The underlying contoured map is annual mean surface heat flux (W m^{-2}) from the atmosphere to the ocean (positive is ocean heating), from NCEP reanalysis data. (b) Heat transport estimates (PW) for each ocean and summed for the globe where available in all oceans. No error bars are shown because they are difficult to estimate (see section 2c), but a reasonable assumption is 10%–20% or ±0.1 to 0.2 PW.

TABLE 1. Total meridional heat transports (1 PW = 1×10^{15} W) and transport components: volume transports (Sv $\equiv 1 \times 10^6$ m^3 s^{-1}), "temperature transports" (1 PWT = 1×10^{15} W). Positive (negative): ocean gaining (losing) heat.

Section	Dates	Ship	Total heat transport (PW)	Total volume transport (Sv)	Geostrophic volume transport (Sv)	Geostrophic temperature transport (PWT)	Ekman volume transport (Sv)	Ekman temperature transport (PWT)
Atlantic 59°N	Mar–Apr 1962	*Erika Dan*	0.70	−2.07	−0.92	0.73	−1.15	−0.04
Atlantic 53°N	Jan–Feb 1962	*Erika Dan*	0.62	−2.01	0.57	0.72	−2.58	−0.10
Atlantic 45°N	Apr 1957	*Discovery*	0.62	−2.00	0.91	0.77	−2.90	−0.16
Atlantic 36°N	Jun–Jul 1981	*Atlantis II*	0.86	−1.94	1.44	1.14	−3.37	−0.28
Atlantic 32°N	1957 to 1986	Several	−0.01[c]	−2.00	−0.46	0.13	−1.54	−0.14
Atlantic 24°N	Aug–Sep 1981	*Atlantis II*	1.28	−1.62	−7.57	0.72	5.94	0.56
Atlantic 8°N	May 1957	*Crawford*	0.73	−2.03	−12.72	−0.40	10.68	1.13
Atlantic 8°S	Mar 1957	*Crawford*	−0.22[c]	−2.00	10.88	1.10	−12.82	−1.32
Atlantic 11°S	Mar–Apr 1983	*Oceanus*	−0.38[c]	−2.00	9.60	0.79	−11.60	−1.17
Atlantic 16°S	Apr 1957	*Crawford*	0.61	−2.00	6.64	1.44	−8.63	−0.82
Atlantic 24°S	Oct 1958 Nov 1972	*Crawford* *Melville*	0.37	−2.00	1.81	0.70	−3.80	−0.32
Atlantic 32°S	Apr–May 1959 Nov 1972	*Atlantis* *Melville*	0.23	−1.35	−2.35	0.15	0.99	0.08
Atlantic 40°S	1925–83	Several	−0.03[c]	−1.92	−9.14	−0.35	7.23	0.32
Pacific 47°N	Aug–Sep 1985	*T. Thompson*	0.01	1.94	7.10	0.19	−5.17	−0.17
Pacific 35°N	1965–91	Several	0.77	1.98	6.29	1.09	−4.32	−0.32
Pacific 24°N	Mar–Jun 1985	*T. Thompson*	0.81	1.85	−9.48	−0.26	11.34	1.07
Pacific 10°N	Feb–May 1989	*Moana Wave*	1.25	2.11	−37.43	−3.03	39.55	4.28
Pacific 28°S	Jun–Jul 1967	*El Tanin*	−0.03 − 0.40[a] = −0.43	9.35	13.76 −8[a] −1.35[b]	0.35 −0.40[a] 0.0[b]	−4.41	−0.38
Pacific 43°S	Mar–May 1967	*El Tanin*	0.45 − 0.40[a] = 0.05	9.35	1.54 −8[a] −1.35[b]	0.05 −0.40[a] 0.0[b]	7.82	0.39
Indian 32°S	Nov–Dec 1987	*Discoverer*	−0.99 + 0.40[a] = −0.59	−8.0	−10.17 8[a]	−1.12 0.40[a]	2.17	0.13
Pacific 28°S	Jun–Jul 1967	*El Tanin*	0.002 − 0.50[a] = −0.50	11.35	15.76 −10[a] −1.35[b]	0.38 −0.50[a] 0.0[b]	−4.41	−0.38
Pacific 43°S	Mar–May 1967	*El Tanin*	0.47 − 0.50[a] = −0.03	11.35	3.53 −10[a] −1.35[b]	0.08 −0.50[a] 0.0[b]	7.82	0.39
Indian 32°S	Nov–Dec 1987	*Discoverer*	−1.02 + 0.50[a] = −0.52	−10.0	−12.17 10[a]	−1.15 0.50[a]	2.17	0.13

[a] Indonesian Throughflow transports. Temperature transport from Vranes et al. (2002) (0.50 PWT for 10 Sv at 15°C, adjusted down to 0.40 PWT for 8 Sv assumption). The total meridional "heat transports" are net surface heat flux out of the region enclosed by the sections plus throughflows into the ocean north of the zonal section.

[b] Bering Strait transports assumed for South Pacific sections. (Bering Strait transport for other Pacific and all Atlantic sections is equal to the total volume transport.) Heat transports including Bering Strait assume 0 PWT temperature transport.

[c] Apparent problems with these total heat transport estimates because of the geostrophic velocity distribution. See Appendix C.

ITF observations and with RAtl's −1.35 Sv net southward transport at 30°S in the Atlantic (due to the Bering Strait), RPac's South Pacific transports were adjusted upward to a total meridional transport of 9.35 Sv across 28° and 43°S, through a uniform adjustment to velocities at all points on the sections. This adjustment reduces the southward temperature transport and the estimated heat loss in the Pacific north of the sections (Table 2).

RAtl assumed about −2 Sv southward through each Atlantic section from the Bering Strait, although his actual net transports were not the same on each section and were generally less than 2 Sv (Table 1). The primary calculations here use RAtl and RPac's exact Bering Strait transports for each section. Sensitivity to reducing the Bering Strait transport on the primary subtropical sections to 0.8 Sv (and 0.0 Sv as an extreme), with a uniform velocity adjustment for each zonal section, was checked and found to be small (Table 3).

To include Ekman transport in RAtl and RPac, the geostrophic velocities were adjusted uniformly at all points on the sections such that the net geostrophic transport (plus Bering Strait and ITF transports) balances the Ekman transport. Hellerman and Rosenstein's (1983) annual averaged wind stresses were used. The mean, minimum, and maximum absolute value velocity adjustments for all 19 adjusted sections were 0.027, 0.007, and 0.062 cm s^{-1} (appendix C). For comparison, transports using the NCEP winds are considered in ap-

TABLE 2. Sensitivity of South Pacific and Indian Oceans heat flux convergence to ITF transport. 4 Sv ITF from Reid (1997) and Reid (2002) choices for Pacific and Indian Oceans. 8 Sv ITF from Robbins and Toole (1997) choice for Indian Ocean. 10 Sv ITF from recent observations (Vranes et al. 2002). 1 Sv Bering Strait from Reid (1997) choice for Pacific, and from observations (Roach et al. 1995). 1.35 Sv Bering Strait to match Reid (1994) net transport across 32°S in Atlantic.

Section	Assumed ITF and Bering Strait transports (Sv)	Geostrophic plus Ekman temperature transport (PWT)	ITF temperature transport (PWT)*	Total heat flux convergence (PW) (positive: ocean gains heat north of section)
Pacific 28°S	10, 1.35	0.002	−0.50	−0.50
Pacific 43°S	10, 1.35	0.47	−0.50	−0.03
Indian 32°S	10	−1.02	0.50	−0.52
Pacific 28°S	8, 1.35	−0.03	−0.40	−0.43
Pacific 43°S	8, 1.35	0.44	−0.40	0.05
Indian 32°S	8	−0.99	0.40	−0.59
Pacific 28°S	4, 1	−0.11	−0.20	−0.31
Pacific 43°S	4, 1	0.40	−0.20	0.20

* 0.50 PWT at 15°C and 10 Sv (Vranes et al. 2002), adjusted down for 8 and 4 Sv assumptions.

pendix B. The error due to wind climatology is small in most regions except the North Pacific, where it is the largest source of error (section 2c).

Temperatures were assigned to the Ekman transport from the Levitus and Boyer (1994) annual mean climatology. Temperatures at variously 10–50 m were used to partially assess Ekman temperature transport uncertainty (not presented). Temperature at 30 m was chosen, with little difference from calculations made using 10 m.

The steps to produce the geostrophic velocities were 1) obtain the datasets from J. Reid, (1998, personal communication) in order to have identical quality control and data gap filling, 2) calculate station pair transports using Reid's geostrophic reference velocities, 3) adjust the velocities uniformly for a given station pair to match Reid's volume transport for the same station pair (small adjustments, necessitated by differing methods of vertical interpolation to calculate dynamic height at each standard depth), and 4) compute the total Ekman volume transport for each section, divide by the total area of the vertical section, and adjust the velocities at each point by this amount. These adjusted velocities were then used in the integrals of Eq. (1). For sensitivity to ITF or Bering Strait transports, the adjustments to velocities on a given section were made uniformly as for the Ekman adjustment. Reid calculated transport to the deepest common level of each station pair. This practice was followed here to stay close to his original results. Therefore no ''bottom triangle'' transports are included, with the main impact on the meridional overturning streamfunctions (Talley et al. 2002, manuscript submitted to *J. Climate*, hereinafter TRR).

c. Error assessment

Errors are difficult to estimate because there is no quantitative error assessment in the RAtl and RPac circulations. Total heat transports are presented here to show their consistency with previous calculations, many with various error estimates. Test calculations were also made to assess sensitivity of total and component transports to wind and Ekman layer temperature choices (appendix B), ITF and Bering Strait transport choices (Tables 1, 2, and 3), subduction density choices (South Atlantic), and distribution of balancing mass within layers.

Errors in the total heat transport are due to 1) error in the mean circulation, assumed ITF transport, and mean Ekman transport; and 2) steady-state assumption for the circulation and applicable Ekman transport. After trying many different approaches to the calculations (different reference level approaches, ways to match Reid's transports, use of various wind climatologies, etc.), and comparing these heat transports with previously published estimates, I conclude that total heat transport error is 10%–20% (up to 0.2 PW), except at

TABLE 3. Subtropical Pacific and Atlantic heat transport sensitivities to Bering Strait transport choice.

Section	Reid (1994, 1997) Bering Strait transport (residual section transport)	Total heat transport (PW) from Table 1, with Reid Bering Strait transports	Total heat transport with 0.8 Sv Bering Strait transport (Roach et al. 1995)	Total heat transport with 0 Sv Bering Strait transport
Pacific 24°N	1.85 Sv	0.81 PW	0.80 PW	0.78 PW
Pacific 28°S	1.0 Sv*	−0.49 PW	−0.50 PW	−0.51 PW
Atlantic 24°N	−1.62 Sv	1.28 PW	1.30 PW	1.31 PW
Atlantic 32°S	−1.35 Sv	0.23 PW	0.24 PW	0.26 PW

* Reid (1997) assumed 5 Sv net, arbitrarily assigned as 3 Sv Indonesian Throughflow and 2 Sv Bering Strait. This has been reassigned here as 4 Sv ITF and 1 Sv Bering Strait to compute total heat transports.

10° and 24°N in the Pacific, where Ekman transport choices lead to much larger errors (appendix B). [Macdonald (1998) reports error in her inverse model heat transports of ±0.2 to 0.3 PW.] Total heat transports on 4 (all Atlantic) of the 20 sections were extremely inconsistent with previous estimates, by much more than 0.2 PW. Indicators for major problems on three of these sections were very sparse vertical sampling resolution and numerous nonsynoptic cruises (appendix C). These sections are omitted from the figures.

The ITF volume transport range from 4 to 10 Sv affects the South Pacific and Indian heat transports (flux convergence) at the level of 0.1 PW (Table 2), assuming that the ITF temperature transport itself is held fixed at the observed value of 0.5 PWT. If the ITF temperature transport is also varied proportional to the volume transport assumption (Table 2), the total heat transport convergence varies by an additional 0.1 PW (Table 2). Variations in Bering Strait volume transport from 0 to 2 Sv have a negligible effect on heat transport (flux convergence) (Table 3).

Dependence of heat transports on the wind climatology used for Ekman transport is examined by comparing the Hellerman and Rosenstein (1983) and NCEP datasets (appendix B). The resulting differences are less than 0.03 to 0.08 PW at most sections. However, the net heat transport differs by 0.9 and 0.2 PW at 10° and 24°N in the Pacific. There is ample reason to expect that the NCEP and other modern wind climatologies are better than Hellerman and Rosenstein (Harrison 1989) and thus should be used in future analyses of these transports.

The steady-state assumption is being examined by numerous authors using repeat hydrography. Most inverse model error analyses do not include this error source because there is little repeat hydrography. At 24°N in the North Atlantic, Lavin et al. (1998) found little change in net heat transport despite striking changes in temperature throughout the water column. Also at 24°N, Baringer and Molinari (1999) estimated a 0.4 PW annual cycle in the baroclinic heat transport (see appendix A). How this translates to uncertainty in the net heat transport is not clear since other components of the heat transport also have annual cycles. At 24°N in the North Pacific, Roemmich et al. (2001) estimated an interannual variation of 0.3 PW. The steady-state assumption for the Ekman component was examined in models by Jayne and Marotzke (2001), who concluded that seasonal variation in the Tropics can have a major effect on heat transports there but poleward of 20°, single section estimates with climatological wind stress are reasonable.

Error in the component (shallow, intermediate and deep) heat transports arises from 1) assigning the maximum subduction density, 2) assigning the mass-balancing flow components (e.g., warmest water or proportion of full layer in, say, the Gulf Stream to balance the interior and Ekman flows), and 3) choice of isopycnal layer interfaces for the deeper overturns. The first has little impact on the net shallow overturn, since winter surface densities are reasonably well known. The assignment of partial components is examined for each subtropical section and leads to the greatest uncertainty in shallow overturn heat transports. For the intermediate and deep overturns, layer interface choices impact the layer transports and hence bias the individual water mass transformation estimates. Interfaces were chosen to maximize the northward or southward transports in layers, and hence different isopycnals were used for each ocean. On the other hand, the true deep transformations also involve lateral cells within isopycnal layers, as can be seen clearly in the salinity distributions on isopycnals in RAtl and RPac; for instance, deep layers may contain both northward-flowing Circumpolar Deep Water and southward-flowing local Deep Water with slightly different temperatures. These finer points have not been considered here, although these deep lateral cells do contribute to Bryden and Imawaki's (2001) horizontal transport (appendix A) and are one source of the difference between the shallow overturning heat transport calculated here and the top-to-bottom horizontal transport.

3. Total heat transports (heat transport convergence)

Total meridional heat transports, their component temperature transports and the ITF and Bering Strait closures where required to balance mass are listed in Table 1 and summarized in Fig. 1. The Atlantic and Pacific heat transports are reasonably consistent, within the error in Macdonald (1998), with other direct estimates (Table 4), many using the same datasets and regional inverses or reference velocity analyses (Hall and Bryden 1982; Bryden et al. 1991; Roemmich and Wunsch 1985; Roemmich and McCallister 1989; Wijffels et al. 1996; Macdonald 1998; Ganachaud and Wunsch 2000; Holfort and Siedler 2001; reviewed by Bryden and Imawaki 2001).

The expected northward heat transports are found in the Atlantic, with a maximum in the midlatitude North Atlantic. In the South Atlantic, the northward heat transport increases toward the equator, reflecting net heating between the sections. The heat transport of 0.23 PW at 32°S is indistinguishable from Rintoul's (1991) 0.25 PW and Sloyan and Rintoul's (2001a) 0.28 PW. The South Atlantic transports are consistent with Holfort and Siedler's (2001) estimates (except where the calculations here failed completely; see section 2c, Table 1, and appendix C). The 8°N estimate of 0.75 PW is considerably larger than Friedrichs and Hall's (1993) 11°N estimate of 0.3 PW for the month of their observations, but smaller than the maximum that they estimate for annual mean winds and western boundary current strength. The 24°N estimate of 1.3 PW is similar to the 1.2 PW of Hall and Bryden (1982), Roemmich and Wunsch (1985) and Lav-

TABLE 4. Total heat transport comparisons.

Section	Total heat transport (PW) or temperature transport (PWT)	Macdonald (1998)	Individual references
Atlantic 59°N	0.70 PW	—	
Atlantic 53°N	0.62 PW	—	
Atlantic 45°N	0.62 PW	0.65 PW	0.27–0.62 PW (Koltermann et al. 1999)
Atlantic 36°N	0.86 PW	1.01 PW	0.8 PW (Roemmich and Wunsch 1985) 1.2 PW (Sato and Rossby 2000) 0.47 to 1.29 PW (Koltermann et al. 1999)
Atlantic 32°N	−0.01 PW**	—	
Atlantic 24°N	1.28 PW	1.07 PW	1.2 PW (Hall and Bryden 1982) 1.2 PW (Roemmich and Wunsch 1985) 1.27, 1.20, 1.33 PW (Lavin et al. 1998) 1.38 to 1.54 PW (Koltermann et al. 1999)
Atlantic 8°N	0.73 PW	1.39 PW	0.3 PW (Friedrichs and Hall 1993) 1.1 PW (Friedrichs and Hall 1993)
Atlantic 8°S	−0.22 PW**	—	—
Atlantic 11°S	−0.38 PW**	0.89 PW	0.48 to 0.53 PW (Holfort and Siedler 2001)
Atlantic 16°S	0.16 PW	—	0.59 PW (Holfort and Siedler 2001)
Atlantic 24°S	0.37 PW	0.33 PW	0.33 PW (Holfort and Siedler 2001)
Atlantic 32°S	0.23 PW	0.49 PW	0.25 PW (Rintoul 1991) 0.28 PW (Sloyan and Rintoul 2001a) 0.29 PW (Holfort and Siedler 2001)
Atlantic 40°S	−0.03 PW**	—	0.37 PW (Holfort and Siedler 2001)
Pacific 47°N	0.01 PW	0.45 PW	−0.09 PW (Roemmich and McCallister 1989)
Pacific 35°N	0.77 PW	—	−0.16 PW (Reommich and McCallister 1989)
Pacific 24°N	0.81 PW	0.44 PW	0.75 PW (Roemmich and McCallister 1989) 0.76 PW (Bryden et al. 1991)
Pacific 10°N	1.25 PW	0.44 PW	0.7 PW (Wijffels et al. 1996)
Pacific 28°S*	−0.43 PW (−0.03 PWT at 28°S and −0.40 PWT ITF)	— −0.04 PWT	−0.18 PW (Wunsch et al. 1983, no ITF) −0.75 PW (Wijffels et al. 2001, 32°S) 0.13 PWT (Sloyan and Rintoul 2001a, 32°S) 0.43 PWT (Tsimplis et al. 1998, 32°S with ITF)
Pacific 43°S*	0.05 PW (0.45 PWT at 43°S and −0.40 PWT ITF)	— 0.26 PWT	−0.03 PW (Wunsch et al. 1983, no ITF)
Indian 32°S*	−0.59 PW (−0.99 PWT at 32°S and 0.40 PWT ITF)	— −1.30 PWT	−0.42 PW (Robbins and Toole 1997) −0.87 PWT (Sloyan and Rintoul 2001a)

* Includes 8 Sv ITF (Table 2).
** Apparent problems with these heat transports (appendix C).

in et al. (1998), all based on different occupations of the section. The 36°N estimate of 0.9 PW agrees well with Roemmich and Wunsch's 0.8 PW, but is lower than Sato and Rossby's (2000) 1.2 PW. The dip in northward heat transport at 45°N, suggesting local heat gain, is within the 0.1 PW overall sensitivity of the transports and is probably not real. [Net surface heat loss between 53° and 59°N is 0.1–0.2 PW based on many air–sea flux estimates, summarized recently by Macdonald (1998)].

The northward heat transport of 0.8 PW at 24°N in the North Pacific compares well with Roemmich and McCallister's (1989) and Bryden et al.'s (1991) direct estimates of 0.75 and 0.76 PW using the same dataset and wind climatology. Various indirect estimates, such as Trenberth and Caron's (2001) 0.73 PW (see Bryden and Imawaki 2001), are also comparable. Roemmich et al. (2001) used partial-depth, repeat expendable bathythermograph (XBT) surveys to assess seasonal and interannual variability in heat transport in this region. Their mean heat transport is again 0.76 PW, but variations are large, up to 0.3 PW. On the other hand, using global inverse models, Macdonald (1998) and Ganachaud and Wunsch (2000) obtained only 0.45 and 0.5 PW at 24°N, respectively. If NCEP winds are used here (appendix B), the heat transport drops to 0.6 PW, closer to Macdonald's based on similarly weaker Ekman transport (European Centre for Medium-Range Weather Forecasts; ECMWF). The 10°N heat transport estimate of 1.25 PW is larger than Wijffels et al.'s (1996) 0.7 PW and Trenberth and Caron's (2001) ~0.9 PW, but within the error estimates of both. Macdonald (1998) again obtained a much lower value of 0.44 PW, with ECMWF winds. With NCEP winds (appendix B), the heat transport is reduced to 0.36 PW. The 10°N estimate has by far the largest error in this analysis. The large sensitivity to Ekman transport at these two North Pacific sections is probably due to the shallowness of the overturning cells that transport the heat (Wijffels et al. 1996), and also the sheer length of the sections.

The South Pacific and Indian transports are made complicated by the ITF contribution. The assumed ITF temperature transport is 0.50 PWT (10 Sv at 15°C from Vranes et al. 2002). This is adjusted downward in the

core calculations to a volume transport of 8 Sv at 15°C, hence 0.40 PWT. This is included in the total heat convergence into the Indian Ocean of −0.59 PW (Fig. 1 and Table 1). When the observed 10 Sv ITF transport is used and the Indian 32°S transport is increased to 10 Sv southward (my own adjustment) (Tables 1 and 2), the net heat transport is reduced to −0.52 PW. These numbers are very sensitive to the ITF temperature transport and thus are likely not significantly different from RTInd's −0.42 PW, with a very different assumption of 24°C for the ITF and different constraints on the Agulhas Current velocities. The total temperature transport across 32°S in the Indian Ocean is −0.99 PWT, similar to Sloyan and Rintoul's (2001a) −0.87 PWT.

Net heat transports (heat convergences) in the South Pacific at 28° and 43°S, including the ITF transport for closure, assuming 8 Sv, are −0.43 and 0.05 PW (Table 1). The absolute value of these transports depends strongly on the choice of ITF temperature transport, but the difference between them, which is the net surface heat flux between them, is robust. With no leakage out of the Pacific through the ITF or Bering Strait in their inverse calculation, Wunsch et al. (1983) obtained heat transports at 28° and 43°S of −0.18 and −0.03 PW, with the same pattern of more southward heat flux across 28°S than across 43°S. Macdonald's (1998) pattern was similar, with −0.04 and 0.26 PWT of temperature transport across 28° and 43°S, hence with about one-half the heat loss for the area between the two sections as computed here. Sloyan and Rintoul's (2001a) temperature transport for the recent WOCE section at 32°S lies between the 28° and 43°S estimates here. On the other hand, the Wijffels et al. (2001) estimate of −0.75 PW for 32°S is much larger.

The net heat transport across 28°–32°S for all three oceans is estimated to be −0.80 PW. If the 43°S section in the Pacific is used instead of 28°S, the net southward heat transport into the Southern Ocean is reduced to −0.3 PW because −0.5 PW is lost to the atmosphere in the South Pacific's subtropical gyre.

4. Shallow, intermediate, and deep overturning components

In the shallow gyre overturn the western boundary currents move warm water poleward. This is cooled (mainly in the western boundary current separation areas) and then subducted as it returns equatorward. The shallow subduction provides a meridional overturn and poleward heat transport, and should exist as long as there are anticyclonic subtropical gyres, regardless of the presence or strength of deeper overturn at higher latitudes. The various components of shallow, intermediate, and deep overturn in terms of water masses were described in Talley (1999).

The densest subducting subtropical water is defined here as the base of the shallow overturn. The maximum subduction density is the maximum winter density at the subtropical–subpolar gyre boundary, determined by the zero of Sverdrup transport. This choice has strong basis in observations in the Northern Hemisphere (e.g., Yuan and Talley 1992; McCartney 1982). The winter surface density in the Northern Hemisphere was obtained from the Levitus and Boyer (1994) climatology. Because Southern Hemisphere winter station data are so sparse, the maximum winter density was estimated from the historical National Oceanographic Data Center station data (e.g., Talley 1996) rather than from the climatology. Hellerman and Rosenstein's (1983) annual mean winds were used to compute wind stress curl and Sverdrup transport. Other wind climatologies yield nearly the same zero curl and Sverdrup transport and hence the same choice of maximum winter subtropical gyre surface density.

The principal subtropical zonal sections used were the standard locations at 24°N and about 30°S (Fig. 2). As described in Talley (1999), mass was balanced in the subducting part of the gyre using the interior geostrophic flow between the surface and the densest subducted isopycnal, the poleward Ekman transport across the sections, and whatever portion of the western boundary current was required to balance mass. All of the Ekman transport is assumed to remain in the subducting subtropical gyre. In four of the five western boundary currents (Gulf Stream, Kuroshio, East Australia Current, and Agulhas), there was more poleward transport in this shallow layer than needed to balance the Ekman and interior equatorward geostrophic transports and the Indonesian/Bering Strait throughflows if applicable. As a measure of sensitivity to the arbitrary choice of which parts of the western boundary currents to choose for mass balance, two different choices were made for these four basins: 1) using only the lightest, warmest part of the western boundary current upper layer (yielding an upper limit on the poleward shallow heat transport) and 2) distributing the balancing mass uniformly over the full shallow isopycnal layer (yielding a lower poleward heat transport). In contrast, in the South Atlantic's upper layer, the southward Brazil Current transport is smaller than the equatorward Ekman and interior geostrophic (including the Benguela) transports. Mass balance was achieved by excluding a portion of the northward Benguela Current at the eastern boundary in the shallow gyre. The excluded shallow portion of the Benguela arcs northwestward through the South Atlantic to South America and then northward into the Tropics and on into the North Atlantic (see surface circulation maps in RAtl), thus balancing the net southward flow in the underlying deep water layers (e.g., Gordon 1986; Broecker 1991; Schmitz 1995).

The Southern Hemisphere shallow overturns present two special difficulties: 1) connection of the Indian and Pacific through the Indonesian archipelago (ITF) and 2) connection of the Atlantic and Indian subtropical gyres south of Africa (e.g., Talley 1996, 1999). It is useful to separate the heat transport associated with the

warm ITF from the poleward heat transport of the local subtropical gyre overturns in the Indian and South Pacific Oceans. The southward transport in the upper layer of the Agulhas is large enough to contain all of the ITF 8 Sv and all of the Indian Ocean subtropical gyre interior plus Ekman. This assumption yields a minimum (northward) heat transport (heat loss within the northern Indian Ocean) associated with the ITF and therefore a maximum southward heat transport for the local subtropical gyre. For the northward flow across 28°S in the South Pacific, I used two separate assumptions: 1) that the Indonesian/Bering Strait throughflows are within the northward flow of the upper layer (interior subducting waters), or 2) that these throughflows are split between the upper layer and the rest of the water column (Tables 5a and 6). Sensitivity to these assumptions is discussed in section 4a, as is the Atlantic–Indian connection.

Heat transports associated with intermediate and deep water transformation were calculated by zonally averaging mass and temperature transports in isopycnal layers. (Reference pressures for the isopycnal layers were changed every 1000 m, following RAtl and RPac.) The shallow overturning transports, determined as above, were subtracted from the associated near-surface layers. Any remaining volume transport in the shallow layer was then assumed to be transformed into denser water. It was assumed that transformation occurs to the nearest possible density class and not, for instance, to the densest possible water when downwelling or to the surface when upwelling.

a. Shallow overturning heat transport

Heat transports carried by the closed mass system for the subducting layers of the subtropical gyres for the five basins are given in Tables 5a, 5b, and 6 and Figs. 3–5. The Northern Hemisphere results in Talley (1999) have been recalculated, resulting in small changes.

The maximum winter surface density for the North Atlantic subtropical subduction is 27.3 σ_θ (McCartney 1982), which outcrops far to the northeast where the zero wind stress curl and Sverdrup transport intersect Ireland (Fig. 5a; σ_θ is the potential density relative to the sea surface). The North Pacific maximum subducted density is 26.2 σ_θ (Yuan and Talley 1992) and is encountered in the north central region where the isopycnals swing north to cross the zero wind stress curl. The Indian Ocean maximum subducted density is 26.9 σ_θ (Talley 1999) and is found south of Australia (southeast Indian Subantarctic Mode Water). The South Pacific's maximum subducted density is 27.1 σ_θ, in the southeast Pacific where the zero wind stress curl enters Drake Passage. This is the Antarctic Intermediate Water salinity minimum density (Talley 1996, 1999).

The South Atlantic's subtropical gyre is continuous with that of the Indian Ocean, and so the maximum subducted density is actually 26.9 σ_θ and is located south of Australia. To assign a shallow overturning heat transport to the South Atlantic alone, heat transports were computed assuming mass balance above 26.2 and 26.5 σ_θ as well as 26.9 σ_θ (Table 5b). The South Atlantic's shallow overturning heat transport was insensitive within acceptable error to this choice. Therefore 26.2 σ_θ was chosen somewhat arbitrarily for the overall decompositions in the schematics and maps, since it outcrops entirely within the South Atlantic.

The western boundary current transport in the shallow layer of the North Atlantic, North Pacific, South Pacific, and Indian Oceans is larger than the return transport in the interior and Ekman flow. In each western boundary current, the isopycnal above which there was enough volume transport to exactly balance the Ekman and interior geostrophic flow (Table 5; Figs. 3, 4) was determined by iteration. In the South Atlantic (Table 5b, Fig. 3c) the mass balance problem is the opposite: the southward Brazil Current transport is smaller than the interior and Ekman layer northward transports. Here the easternmost part of the northward Benguela Current was excluded to allow mass balance in the rest of the upper ocean. In the South Pacific, throughput for the ITF and Bering Strait was assumed to lie in the upper layer of the northward interior geostrophic flow. In the Indian, the throughput from the ITF was assumed to be in the upper layer of the Agulhas. Sensitivity to these assumptions is discussed below.

1) NORTH ATLANTIC AT 24°N

In the layer above 27.3 σ_θ (Table 5a; Figs. 2a, 3a), the Gulf Stream carries 29.0 Sv northward, the subtropical gyre carries 18.9 Sv southward, and the Ekman transport is 5.9 Sv northward. Mass balance allocates 13.0 Sv of the Gulf Stream to the shallow overturn. If the least dense (warmest) water in the Gulf Stream balances the interior plus Ekman transport, hence with Gulf Stream water less dense than 25.845 σ_θ, the net heat transport for the shallow overturn is 0.40 PW. This leaves 0.88 PW associated with intermediate and deep water formation farther north. Hence the North Atlantic heat transport is dominated by the denser meridional overturn, as concluded by Roemmich (1980), Roemmich and Wunsch (1985), Hall and Bryden (1982), and more recent studies at 24°N, with the Roemmich studies using the same dataset as here.

Because so much of the upper Gulf Stream continues northward into deep overturn, the uncertainty in the shallow overturn heat transport is much larger than for any other ocean. If the warm balancing flow in the Gulf Stream is spread proportionally over the whole Gulf Stream layer rather than confined to the warmest part, the total shallow heat transport is reduced from 0.40 to 0.09 PW (Table 5a). Roemmich and Wunsch (1985) are the only others who have subdivided heat transports in the same overall way as here. They used the same 24°N dataset and an inverse method and divided the heat transport at 27.4 σ_θ into shallow and deep overturn.

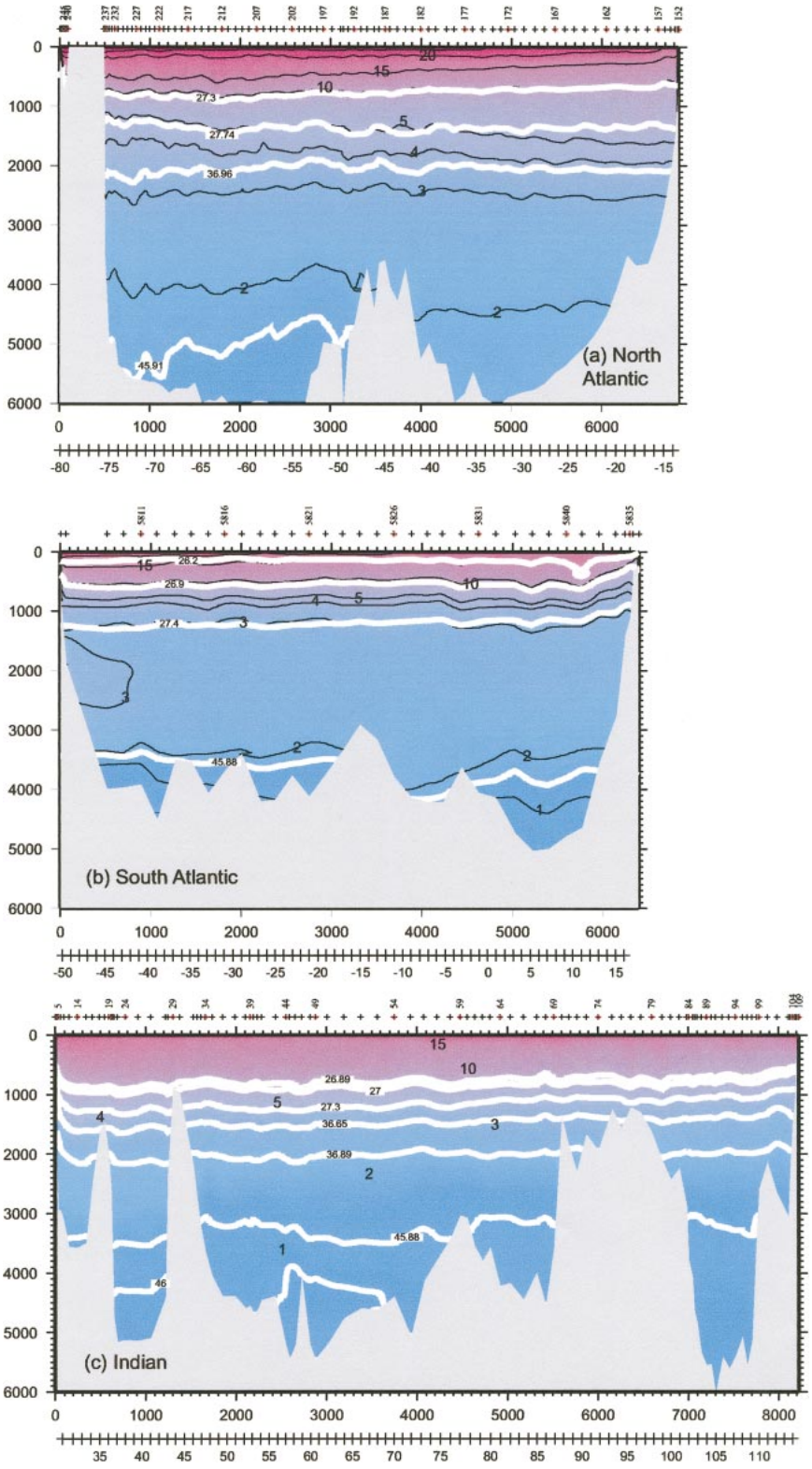

FIG. 2. Vertical sections of potential temperature for each of the primary subtropical zonal sections, with isopycnals (white) used for layer analysis (Tables 7–12). The shallowest isopycnal on each section is the base of subtropical subduction as defined in text. (a) North Atlantic at 24°N, (b) South Atlantic at 32°S, (c) Indian Ocean at 32°S, (d) North Pacific at 24°N, and (e) South Pacific at 28°S.

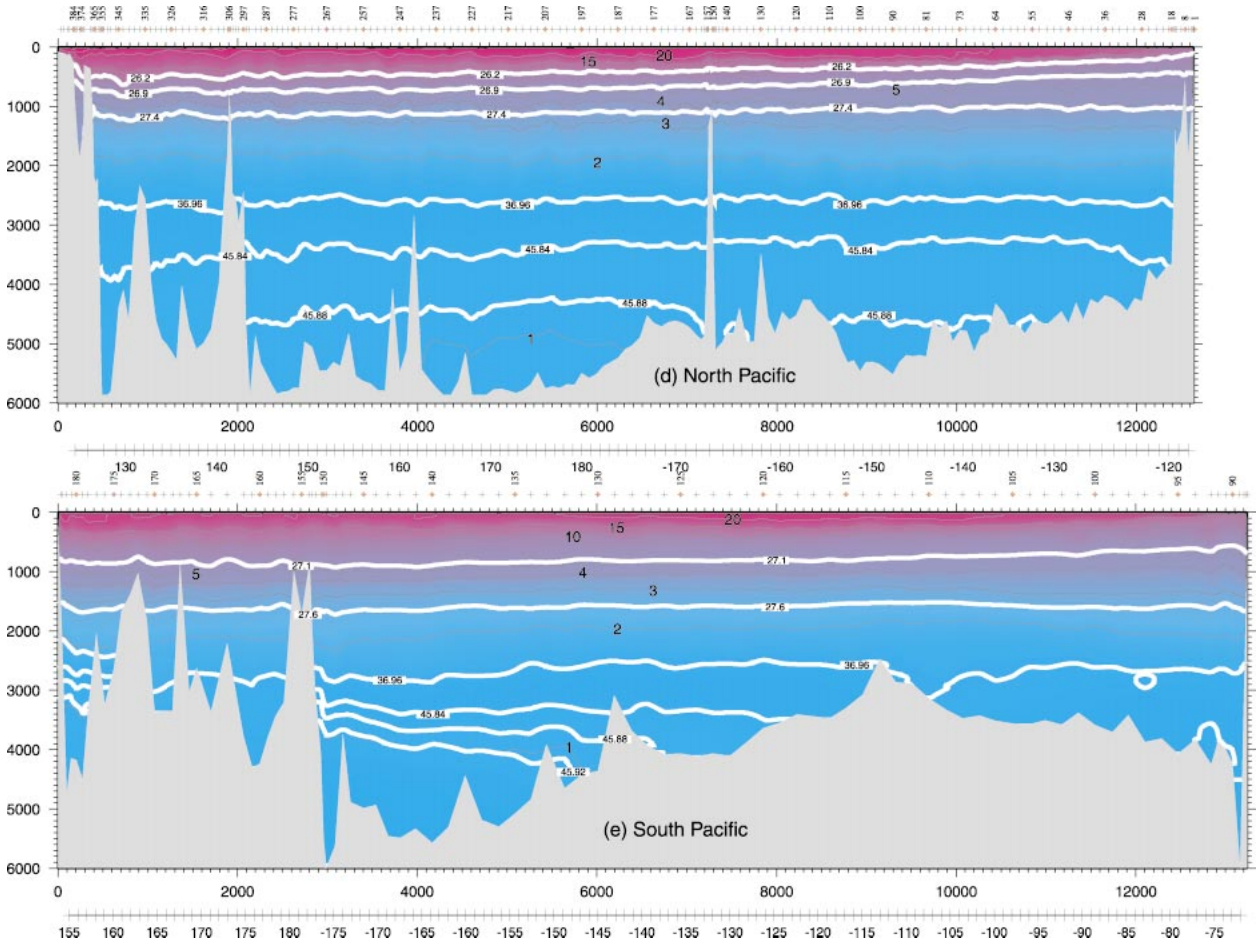

FIG. 2. (*Continued*)

They assumed that the Gulf Stream contribution to the shallow overturn is spread over the full surface layer, yielding 0.1 and 1.1 PW for the shallow and deep overturn, respectively, reassuringly close to the result here (Table 5a).

2) NORTH PACIFIC AT 24°N

In the North Pacific subtropical gyre in the subducting layer above 26.2 σ_θ (Table 5a; Figs. 2b, 3b), the Kuroshio carries 23.4 Sv northward, the subtropical gyre carries 31.5 Sv southward, and the Ekman transport is 11.3 Sv northward. (Ekman transport is approximately double that of the North Atlantic at the same latitude simply because of the greater width of the Pacific). Mass balance is achieved as for the Gulf Stream. The shallow gyre overturn is mass balanced with Kuroshio water less dense than 26.10 σ_θ. This leaves only 3.3 Sv of the shallow layer in the Kuroshio to continue northward into the subpolar gyre, feeding both North Pacific Intermediate Water formation and Bering Strait throughflow. The net heat transport for the shallow overturn is 0.57 PW, which is most of the total heat transport of 0.81 PW. Thus the North Pacific heat transport is dominated by shallow overturn, as concluded previously by Bryden et al. (1991) using the same dataset and a different approach to separating the shallow and deeper overturn (section 5b).

3) SOUTH ATLANTIC AT 32°S

The South Atlantic's subtropical gyre (Table 5b; Figs. 2c, 3c) is connected to the Indian subtropical gyre, leaving an ambiguity in defining the shallow overturning heat transport. Therefore the shallow heat transport was computed for a range of densities, for example, for 26.2 and 26.5 σ_θ (outcropping within the South Atlantic) and for 26.9 σ_θ, the maximum subduction density in the Indian Ocean. Also as described above and shown in Table 5b, regardless of this choice of maximum shallow gyre density, the Brazil Current is too weak to balance the (northward) Ekman transport and northward interior flow. Mass balance was achieved by excluding the easternmost part of the Benguela Current at the eastern boundary from the closed shallow gyre overturn. [This warm portion of the Benguela Current is then included

TABLE 5a. Shallow overturning volume and heat transports for all basins except the South Atlantic. The ''PW'' unit is used for mass-balanced heat transport. ''PWT'' is used for components of heat transport without mass balance (''temperature transport'').

Section	Max subducted density (σ_θ)	1) Ekman volume transport (Sv) and temperature transport (PWT)	2) Total shallow interior geostrophic volume transport (Sv) and temperature transport (PWT)	3) Assumed ITF and Bering Strait portion of interior geostrophic transport (see text)	Total shallow WBC volume transport (Sv) and temperature transport (PWT)	Balancing WBC volume transport (Sv) and dividing density (1 + 2 − 3)	4) WBC temperature transport (PWT) for water lighter than dividing density (for shallow overturn)	* Shallow overturn heat transport (PW) using light WBC water (1 + 2 − 3 + 4)	5) WBC temperature transport (PWT) using portion of full shallow WBC layer (for shallow overturn)	Shallow overturn heat transport (PW) using full WBC layer (1 + 2 − 3 + 5)
Atlantic 24°N	27.3	5.95 Sv 0.56 PWT	−18.95 Sv −1.56 PWT	—	29.02 Sv 2.43 PWT	13.01 Sv 25.75 σ_θ	1.40	*0.40	1.09	0.09
Pacific 24°N	26.2	11.34 Sv 1.07 PWT	−31.52 Sv −2.22 PWT	—	23.40 Sv 1.97 PWT	20.18 Sv 25.95 σ_θ	1.72	*0.57	1.70	0.54
Pacific 28°S	27.1	−4.41 Sv −0.38 PWT	33.67 Sv 1.95 PWT	11.35 Sv 0.66 PWT	−23.99 Sv −1.52 PWT in interior	−17.91 Sv 26.70 σ_θ	−1.31	−0.40	−1.14	−0.23
Pacific 28°S	27.1	−4.41 Sv −0.38 PWT	33.23 Sv 1.92 PWT	9.35 Sv 0.54 PWT in interior	−24.00 Sv −1.52 PWT	−19.49 Sv 26.83 σ_θ	−1.38	*−0.38	−1.24	−0.24
Pacific 28°S	27.1	−4.41 Sv −0.38 PWT	33.23 Sv 1.92 PWT	9.35 Sv (4.82 Sv/0.29 PWT surface and 4.53 Sv/0.07 PWT deep layers)	−24.00 Sv −1.52 PWT	−24.00 Sv 27.1 σ_θ	—	—	−1.52	*−0.26
Pacific 28°S	27.1	−4.41 Sv −0.38 PWT	32.29 Sv 1.88 PWT	5.0 Sv 0.29 PWT in interior	−24.02 Sv −1.53 PWT	−22.88 Sv 27.05 σ_θ	−1.50	−0.29	−1.45	−0.24
Indian 32°S	26.9	2.16 Sv 0.13 PWT	38.4 Sv 2.00 PWT	(−8.00 Sv −0.47 PWT in Agulhas)	−51.7 Sv −3.06 PWT	−40.5 Sv Density not determined	—	—	−2.40	*−0.27

* Transports used in summaries and text.

TABLE 5b. South Atlantic shallow overturning volume and heat transports for varying subduction densities. "Shallow" means the layer from the sea surface to the chosen maximum subduction density (second column).

Section	Max subducted density (σ_θ)	1) Ekman volume transport (Sv) and temperature transport (PWT)	Total shallow geostrophic volume transport (Sv) and temperature transport (PWT)	2) Total shallow Brazil Current (WBC) volume transport (Sv) and temperature transport (PWT)	3) Balancing shallow interior volume transport (Sv) and temperature transport (PWT)	4) Shallow overturning heat transport (PW) (sum of 1, 2, and 3)	Residual shallow Benguela Current volume transport (Sv) and temperature transport (PWT)	Intermediate/ deep overturning heat transport (PW) (total heat transport minus 4)
Atlantic 32°S	26.2	0.99 Sv	3.07 Sv	−6.16 Sv	5.17 Sv	*−0.11	4.06 Sv	0.34
		0.076 PWT	0.079 PWT	−0.526 PWT	0.339 PWT		0.266 PWT	
Atlantic 32°S	26.5	0.99 Sv	1.88 Sv	−8.47 Sv	7.49 Sv	−0.10	2.75 Sv	0.33
		0.076 PWT	−0.007 PWT	−0.669 PWT	0.917 PWT		0.173 PWT	
Atlantic 32°S	26.9	0.99 Sv	6.41 Sv	−11.54 Sv	10.55 Sv	−0.13	5.78 Sv	0.36
		0.076 PWT	0.208 PWT	−0.819 PWT	0.615 PWT		0.314 PWT	

* Transports used in summaries and text.

in the heat transports for the mass-balanced deeper overturns that include this northward warm flow, balanced by the deep southward flow of North Atlantic Deep Water as well as other deep overturning components; see section 4b(3).]

The resulting net shallow overturning heat transport for the South Atlantic is southward, as in every other subtropical gyre, despite the northward total heat transport, the northward Ekman transport, and the use of waters within the same shallow layer for both the Brazil Current and interior flow. This is because the average potential temperature (and salinity) of the northward interior flow is lower than the Brazil Current's temperature (and salinity) in the same density range. The shallow overturning heat transports are reassuringly independent of the assumed maximum subduction density (Table 5b). Thus it appears possible to bound the South Atlantic shallow overturning heat transport. Using 26.2 σ_θ as the primary choice, the Brazil Current geostrophic transport is −6.2 Sv, the Ekman transport is 1.0 Sv, the balancing interior transport is 5.2 Sv, and the residual Benguela Current transport is 4.1 Sv. The (southward) heat transport for the shallow overturn is −0.11 PW. Thus the deep meridional overturn, including northward flow of warm Benguela Current water down through Antarctic Intermediate Water, overturning into North Atlantic Deep Water, must carry 0.34 PW northward. How this is divided between the thermocline and Antarctic Intermediate Water layers is considered in section 4b(4).

4) INDIAN OCEAN AT 32°S

The Indian Ocean's interior geostrophic transport above 26.9 σ_θ is 38.4 Sv northward, its Ekman transport is 2.2 Sv northward, and the ITF is 8.0 Sv into the Indian Ocean (Table 5a; Figs. 2c, 4a). These are balanced by −48.5 Sv southward in the Agulhas above 26.9 σ_θ. (The total Agulhas transport above 26.9 σ_θ is −51.7 Sv. The extra −3.2 Sv must originate as upwelling in the Indian Ocean north of 32°S and eventually feed into deep water formation elsewhere.) Since the transport numbers were supplied by P. Robbins (1999, personal communication), and because there was already ambiguity in assigning a temperature to the outflow of ITF water in the Agulhas, the transports were not iterated to determine the density that would accommodate the −48.5 Sv in the warmest part of the Agulhas. The subtropical gyre shallow overturning heat transport is the sum of the Ekman transport, shallow interior northward transport, and the part of the shallow Agulhas transport required to balance these, not including the ITF portion of the shallow Agulhas. The shallow overturning transport is −0.27 PW, which is poleward as in all other subtropical gyres, with associated heat loss poleward of and heat gain equatorward of 32°S.

Heat is also transported by the closed ITF loop, including 0.40 PWT through the archipelago (adjusted from Vranes et al. 2002, Tables 2 and 6) and −8 Sv

TABLE 6. Heat transports (PW) associated with the ITF and Bering Strait (BS) throughput for the Indian and South Pacific subtropical sections. Temperature of 15°C assumed for the ITF in the Indonesian passages. Temperature transport of 0 PWT assumed for BS.

Section	Total heat transport (PW) (Tables 1 and 3)	Total shallow overturn heat transport (PW) (Table 5)	ITF volume transport (Sv)	1) ITF temperature transport (PWT)	2) Section meridional temperature transport for volume balancing ITF (PWT)	Heat transport associated with ITF (PW) (1 + 2)	3) Section temperature transport for volume balancing 1.35 Sv Bering Strait (PWT)	Heat transport associated with Bering Strait (PW) (3 + 0.0 PWT)
Pacific 28°S	−0.58	−0.52[a]	−10	−0.50	0.57[a]	0.07[a]	0.08[a]	0.08[a]
Pacific 28°S	−0.43	−0.38[a]	−8	−0.40	0.46[a]	0.06[a]	0.08[a]	0.08[a]
Pacific 28°S	−0.43	−0.23[b]	−8	−0.40	0.33[b]	−0.07[b]	0.03[b]	0.03[b]
Pacific 28°S	−0.43	−0.23[c]	−8	−0.40	0.29[c]	−0.11[c]	0.03[c]	0.03[c]
Indian 32°S	−0.59	−0.27	8	0.40	−0.47	−0.07	—	—

[a] Net northward transport assigned to 28°S layer above 27.1 σ_θ.
[b] Net northward transport assigned to northward flow between 165° and 130°W in the layer 27.1–27.6 σ_θ.
[c] Northward transport assigned to northward flow between 165° and 130°W between 27.1 σ_θ and the bottom.

southward in the Agulhas. Where in the Agulhas should the ITF water be assigned? Although the ITF water flows nearly exactly zonally westward across the Indian Ocean (Gordon et al. 1997), when it reaches the western Indian, some may turn northward and be transformed to more saline deeper water. Ignoring this, and assuming that the ITF water remains above 26.9 σ_θ, but assuming only that the 8 Sv is a proportion of the total Agulhas transport above 26.9 σ_θ rather than being the very warmest water, the temperature transport of ITF throughput in the Agulhas is −0.47 PWT. The total ITF-associated heat transport is then very small: −0.07 PW out of the Indian Ocean (Table 6). In a previous version of this manuscript, a temperature of 24°C was chosen for the ITF inflow following RTInd, resulting in a large transport of heat into the Indian Ocean associated with the closed ITF loop. The reduction to nearly zero heat transport when using the newly observed ITF temperature transport is reassuring since otherwise large heat loss would be required in the tropical Indian. If the ITF were assigned to denser, colder layers in the Agulhas, a net heat loss would be required in the northern Indian Ocean, which again seems unlikely.

RTInd decomposed the heat transport along the lines of Bryden and Imawaki (2001). As shown in appendix A, the three heat transport components (''leakage,'' barotropic, and baroclinic) are not exactly equivalent to the ITF, shallow overturn, and deeper overturns computed here.

5) SOUTH PACIFIC AT 28°S

The South Pacific's interior shallow geostrophic transport above 27.1 σ_θ (Table 5a; Figs. 2c, 4b) is 32.3 Sv northward and the Ekman transport is −4.4 Sv southward. The East Australia Current (EAC) carries −24 Sv in this layer, and so the net transport in the upper ocean is 4.8 Sv (northward). The ITF and Bering Strait transports are chosen to be 8 and 1.35 Sv exiting the Pacific, to match the transports across 32°S in the Indian Ocean and 30°S in the Atlantic Ocean, respectively. For one extreme of the heat transport calculations, it is assumed that all of the 9.35 Sv Indonesian and Bering Strait throughflows are in the shallow interior layer. With this choice, the closed shallow overturning gyre includes 23.9 Sv in the interior, −4.4 Sv in the Ekman layer, and −19.5 Sv of the shallow EAC, resulting in a dividing density in the EAC at 26.83 σ_θ. The net shallow overturning heat transport for this mass-balanced gyre is −0.38 PW.

The heat transports (heat flux convergence in the Pacific north of this section) due to the throughput of ITF and Bering Strait waters (Table 6), closed by their temperature transports through the Indonesian archipelago and Bering Strait, are 0.06 and 0.08 PW, if the throughput of ITF and Bering Strait waters is in the upper layer. Thus the average temperature of the inflow is slightly higher than that of the outflows, and there is a small net heat loss within the Pacific associated with this loop. This is indistinguishable from zero, as in the Indian Ocean.

What if the ITF and Bering Strait throughput transports are not contained wholly in the upper layer of the subtropical gyre? It seems reasonable to assume that the net 4.8 Sv in the upper layer partially feeds the ITF and Bering Strait. The remaining 4.5 Sv can be assigned anywhere and was assigned in the previous paragraphs to the upper layer as well. In the deeper layers, the horizontal structure of the transports includes northward flow between 165° and 130°W; in the deepest layers this encompasses the northward Deep Western Boundary Current (maps in RPac). If 4.5 Sv of the ITF/Bering Strait throughput is assigned to this northward flow in the layer 27.1–27.6 σ_θ, the total temperature transport associated with balancing the ITF/Bering Strait throughput across 28°S is reduced to 0.36 PWT (Table 5a). The total heat transport associated with the ITF is then −0.07 PW (Table 6), again small, but now indicating net heat-

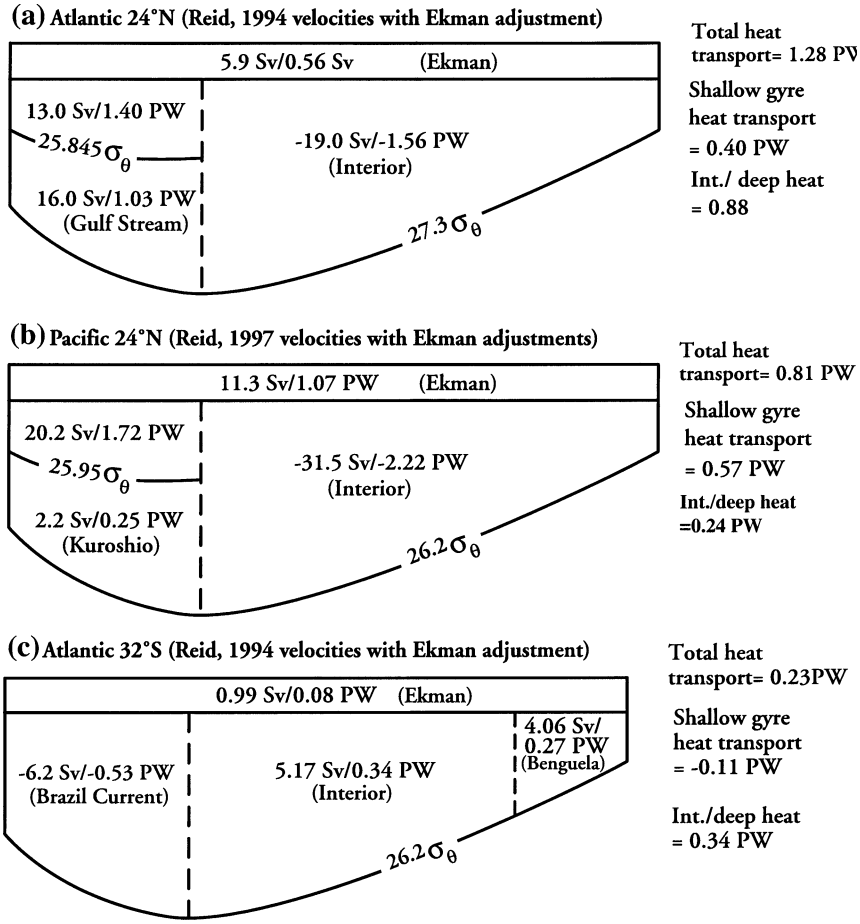

FIG. 3. Schematics of shallow overturning transports in three subtropical gyres: (a) North Atlantic at 24°N, (b) North Pacific at 24°N, and (c) South Atlantic at 32°S. Numbers listed in each portion of each panel are the volume and temperature transports. Each schematic includes the Ekman transport in the layer across the top, the western boundary current transport at the left side, and the interior transport within the right side. Since the North Atlantic and North Pacific western boundary currents (WBCs) carry more water than needed to balance the interior plus Ekman, the densities in the WBCs above which the transports balance are shown. In the South Atlantic, mass balance for the Ekman layer, western boundary current, and interior is achieved by subtracting a portion of the Benguela Current transport in the east.

ing in the Pacific. If the ITF/Bering Strait throughput is assigned to the northward flow from 27.1 σ_θ to the bottom, there is a further slight reduction in its temperature transport and a slightly larger Pacific heat loss of -0.20 PW associated with the ITF throughput.

The shallow overturning gyre heat transport must be recalculated if it is assumed that part of the ITF/Bering Strait flow is in deeper layers since more of the northward interior flow remains in the closed gyre. The entire EAC above 27.1 σ_θ is then used to balance the Ekman and northward interior, and the total shallow overturning heat transport is -0.23 PW. This is smaller than the -0.38 PW calculated when only the warmest part of the EAC was included in the shallow gyre balance (Table 5a), but identical to the shallow gyre heat transport when the EAC balancing transport was distributed over the whole surface layer and hence had a lower mean temperature (Table 5a, last column).

Since there is no a priori reason to select between containment of ITF/Bering Strait throughput entirely within the surface layer or distributed into the surface layer and deeper northward flows, these two calculations give a range for the impact of these flows on the Pacific heat transport from 0.1 PW if contained entirely within the surface layer to -0.1 PW if distributed with depth. Both results are shown in Fig. 5a. The deeper overturning in section 5 is calculated with the deep distribution of ITF/Bering Strait throughput.

6) SUMMARY

Heat transports in the shallow overturning circulations (Fig. 5a) are poleward in each subtropical gyre.

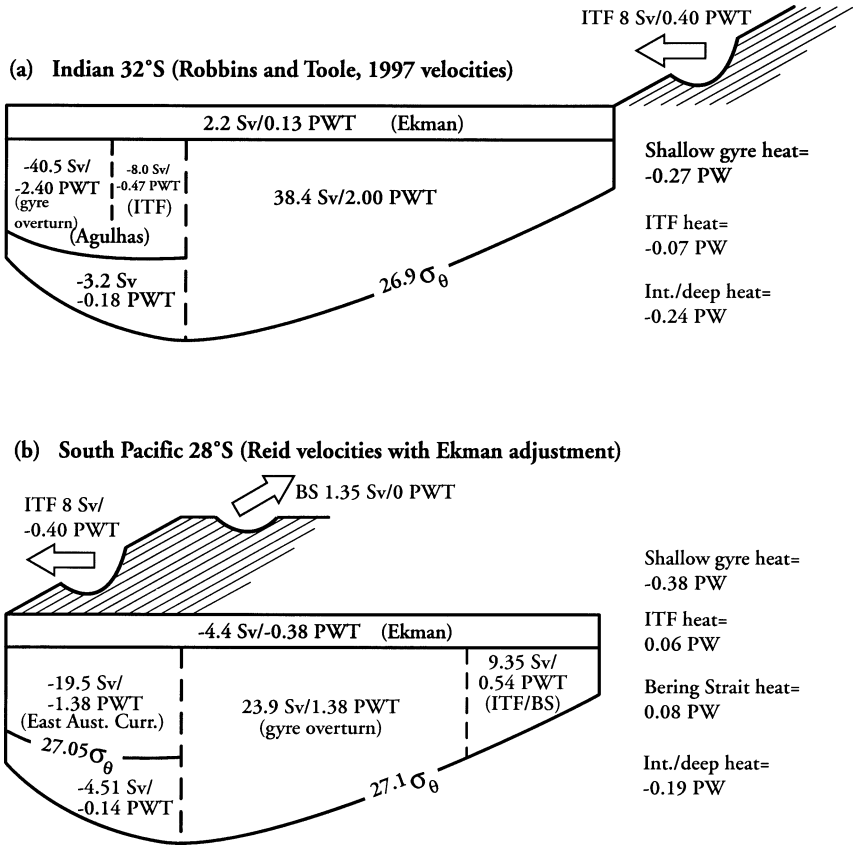

FIG. 4. Shallow overturning transport schematics: (a) Indian Ocean at 32°S and (b) South Pacific at 28°S. Dividing densities in the western boundary currents are as in Fig. 3. ITF and Bering Strait (BS) values are shown, based on Reid (1997) (Pacific) and Robbins and Toole (1997) (Indian Ocean). (See Table 2 for other choices of ITF transports.)

The Northern Hemisphere heat transports are larger than the Southern Hemisphere heat transports, perhaps due to the larger average surface heat loss in the Gulf Stream and Kuroshio separation regions compared with the equivalent Southern Hemisphere regions (Brazil, Agulhas, and East Australia Currents). The heat transport carried by the Indonesian Throughflow is negligible, given the relatively low average temperature of the ITF of 15°C observed by Vranes et al. (2002). This indicates that the average temperatures of ITF, the balancing southward flow in the Agulhas, and the balancing northward flow in the South Pacific's subtropical gyre are about the same.

b. Intermediate and deep overturning heat transports

Heat transports associated with formation, advection, and upwelling of the intermediate, deep, and bottom waters are next calculated from the zonally summed transports in isopycnal layers, as in many previous transport treatments (e.g., Bryden et al. 1991; Macdonald 1998). The shallow overturning transports (section 4a) are subtracted from the total surface layer transports so the remaining surface layer transport is part of the intermediate/deep meridional overturn. Heat transports for each component of the deeper overturn are calculated using volume and temperature transports in isopycnal layers, with layer interfaces chosen to maximize northward or southward transport if appropriate.

The heat transports associated with intermediate water [Labrador Sea Water (LSW) and North Pacific Intermediate Water (NPIW)] and North Atlantic Deep Water (NADW), Pacific Deep Water (PDW), and Indian Deep Water (IDW) creation, and with Lower Circumpolar Deep Water/Antarctic Bottom Water (LCDW/AABW) upwelling in the Tropics (equivalently, LCDW formation in the Southern Ocean) are detailed in the following sections and summarized in Fig. 5b.

1) NORTH ATLANTIC AT 24°N (FIG. 6A AND TABLE 7)

The shallow subtropical gyre overturn accounts for 0.1–0.4 PW of the total heat transport as shown above. The remaining northward transport in the thermocline and Antarctic Intermediate Water (AAIW) layers increases in density in the north and becomes LSW and NADW, at rates of 7.0 and 9.1 Sv, respectively. Also,

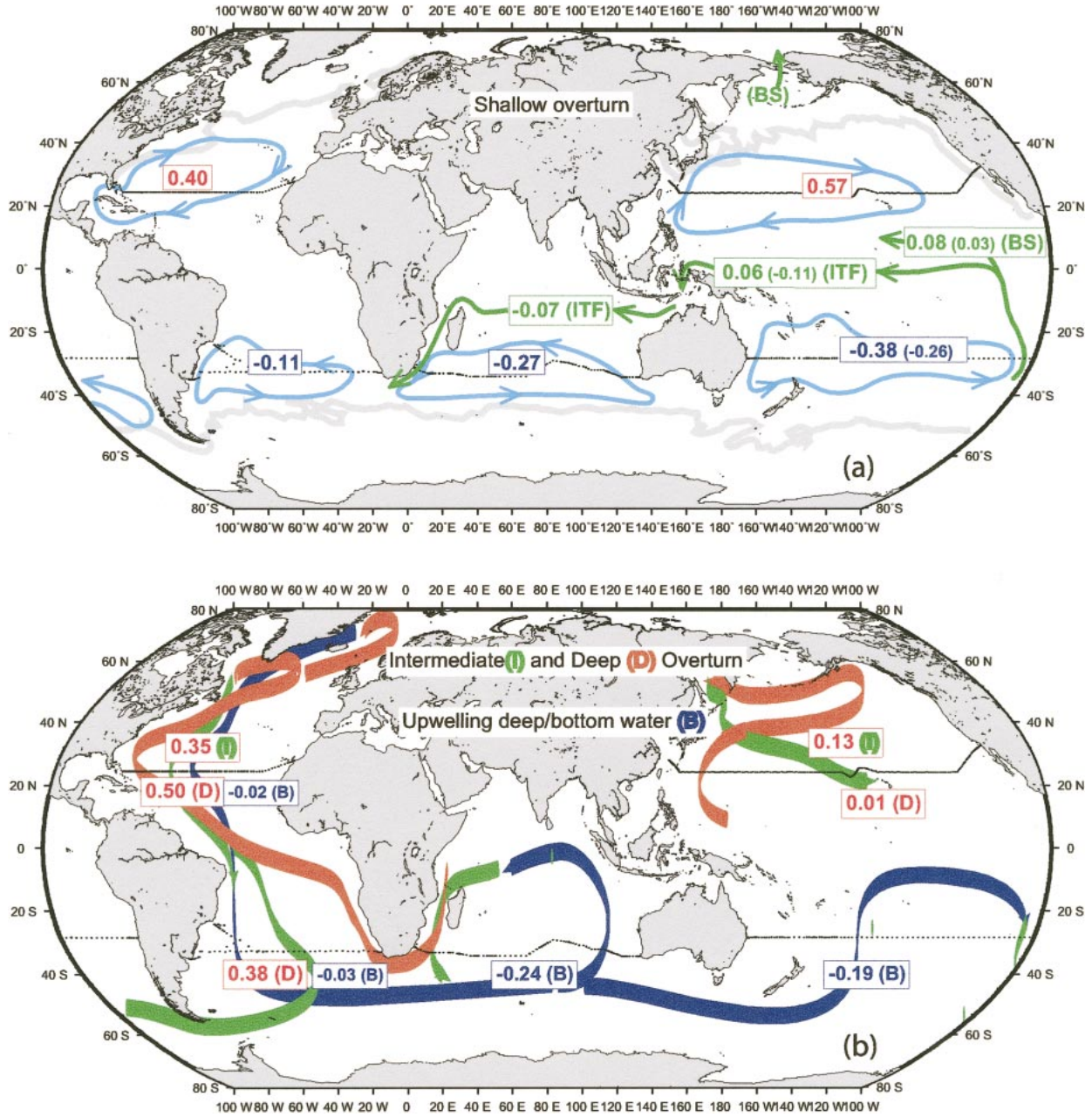

FIG. 5. (a) Shallow overturning heat transports (PW) for each anticyclonic subtropical gyre and those associated with the ITF (asterisked values in Table 5). Red indicates northward; blue indicates southward. Green numbers are heat transports associated with the ITF, including both flow through the passages and across the basin zonal section, hence for balanced mass. In the South Pacific, two gyre and ITF values are given: the first is based on ITF inflow across 28°S entirely within the shallow layer while the second, in parentheses, is based on ITF inflow split between the shallow layer and the 27.1–27.6 σ_θ layer (see text and Table 11). Schematic streamlines for the gyres are based on adjusted geostrophic streamfunctions in Reid (1994, 1997) for the Atlantic and Pacific (from Talley 1999). The underlying light gray contours are the zeros of wind stress curl used to determine the location of maximum winter surface density in each basin. (b) Intermediate (I), deep (D), and bottom (B) water overturning heat transports, based on calculations shown in Fig. 6 and listed in Tables 7–11. Red numbers: northward (>0) transport. Blue numbers: southward (<0) transport. The underlying cartoon of pathways illustrates crudely the direction of large layers involved in the overturning; red: upper ocean; green: intermediate waters; blue: deep and bottom waters.

the 6.7 Sv of AABW upwells into the overlying NADW layer assuming the minimum density change. (This AABW volume transport is larger than the AABW transports on the other Atlantic sections, not shown except for 30°S, where the transport appears to be too low. Lack of continuity in bottom water transports is a problem in the RAtl and RPac analyses, arising from accommodating the large variation in near-bottom sam-

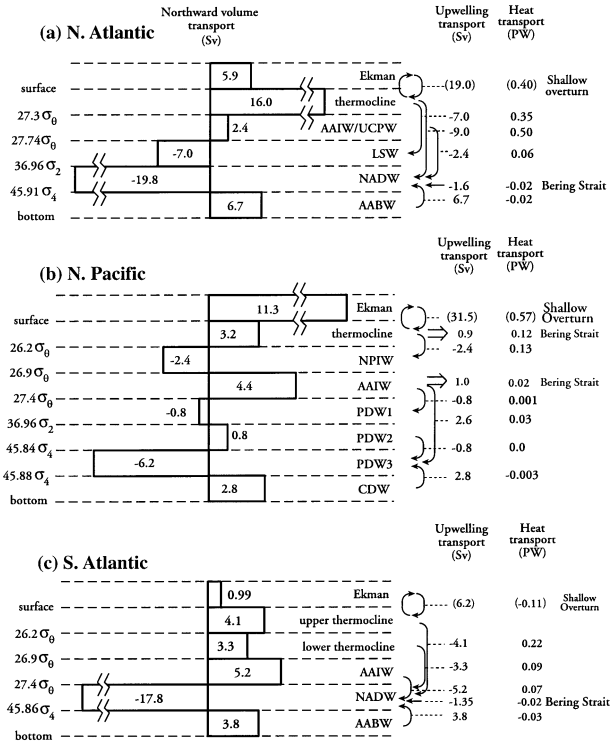

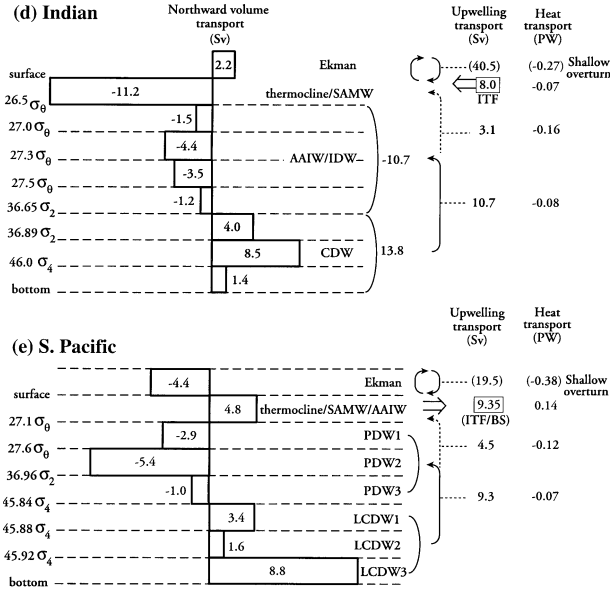

FIG. 6. Meridional overturning transports for the (a) North Atlantic at 24°N, (b) North Pacific at 24°N, (c) South Atlantic at 32°S, (d) Indian Ocean at 32°S, and (e) South Pacific at 28°S. On the left are the densities of the layer interfaces. These were chosen to maximize the northward or southward zonally integrated volume transport in the layers, and so differ from basin to basin. In the center bar graphs are the layer total volume transports, labeled at the right by various water masses: AAIW, LSW, NADW, AABW, NPIW, PDW, LCDW, and IDW. At the right, the net overturning volume transports between layers are shown, and the heat transports that go with these mass-balanced overturns.

FIG. 6. (*Continued*)

pling; see appendix C.) The heat transports associated with LSW/NADW overturn are computed from the temperature transports associated with each of these elements. Thus the LSW overturn carries 0.35 PW, the NADW overturn carries 0.50 PW, and the AABW upwelling carries −0.02 PW. The last is negligible despite the sizeable volume transport because the temperature difference between AABW and NADW is small. Thus LSW formation carries almost as much heat transport as the shallow overturn and NADW formation.

2) NORTH PACIFIC AT 24°N (FIG. 6B AND TABLE 8)

The shallow overturn due to the upper part of the Kuroshio, Ekman transport, and the subducting ther-

TABLE 7. North Atlantic (24°N) zonally averaged overturns.

Layer	Heat transport (PW)	Volume transport (Sv) temperature transport (PWT)	Volume and total heat transport (PW) from conversion to LSW/NADW
Total heat transport (Table 1)	1.28	—	—
Shallow overturning layer (Table 5a)	0.40	18.96 Sv closed circulation	—
Net intermediate–deep overturning heat transport	0.88	—	—
Surface–27.3 σ_θ (thermocline, after shallow overturn subtracted)	—	16.01 Sv 1.03 PWT	6.96 Sv 0.35 PW to LSW 9.05 Sv 0.50 PW to NADW
27.3–27.74 σ_θ (AAIW/UCPW)	—	2.37 Sv 0.087 PWT	2.37 Sv 0.06 PW to NADW
27.74 σ_θ–36.96 σ_2 (LSW)	—	−6.96 Sv −0.100 PWT	—
36.96 σ_2–45.91 σ_4 (NADW)	—	−19.76 Sv −0.184 PWT	—
Bering Strait throughput in NADW layer	—	−1.63 Sv 0 PWT	−1.63 Sv −0.02 PW to NADW
45.91 σ_4–bottom (AABW)	—	6.72 Sv 0.04 PWT	6.72 Sv −0.02 PW to NADW

TABLE 8. North Pacific (24°N) zonally averaged overturns.

Layer	Heat transport (PW)	Volume transport (Sv) and temperature transport (PWT)	Volume and heat transport from conversion to NPIW/PDW
Total heat transport (Table 1)	0.81	—	—
Shallow overturning layer (Table 5a)	0.57	31.52 Sv closed circulation	—
Net intermediate–deep overturning heat transport	0.27	—	—
Surface–26.2 σ_θ (thermocline, after shallow overturn subtracted)	—	3.22 Sv 0.25 PWT	2.37 Sv/0.13 PW to NPIW 0.85 Sv/0.12 PW to Bering Strait
26.2–27.0 σ_θ (NPIW)	—	−2.37 Sv −0.049 PWT	—
27.0–27.6 σ_θ (AAIW/UCDW)	—	4.37 Sv 0.067 PWT	1.00 Sv/0.02 PW to Bering Strait 0.77 Sv/0.01 PW to PDW1 2.59 Sv/0.03 PW to PDW3
27.6 σ_0–36.96 σ_2 (PDW1)	—	−0.77 Sv −0.005 PWT	—
36.96 σ_2–45.84 σ_4 (PDW2)	—	0.80 Sv 0.004 PWT	0.80 Sv/0.0 PW to PDW3
45.84–45.88 σ_4 (PDW3)	—	−6.19 Sv −0.03 PWT	—
45.88 σ_4–bottom (LCDW)	—	2.79 Sv 0.01 PWT	2.79 Sv/−0.003 PW to PDW3

mocline layer accounts for 0.57 PW of the total 0.81 PW. Formation of NPIW is associated with only 2.4 Sv and a heat transport of only 0.13 PW. The remaining northward upper layer transport of 0.85 Sv feeds Bering Strait, joined by 1.0 Sv from upwelling AAIW, since RPac's net Bering Strait transport at 24°N is 1.85 Sv. The total Bering Strait heat transport contribution is 0.14 PW. The negligible remaining 0.03 PW of the total heat transport comes from downwelling of 3.4 Sv of AAIW and 0.8 Sv of middepth PDW into the deepest part of the PDW. Upwelling of the cold, bottommost Circumpolar Deep Water into the PDW is 2.8 Sv with a negligible associated heat transport of −0.003 PW.

Downwelling from middepths to the abyss was obtained in earlier independent analyses of the same dataset (Roemmich and McCallister 1989; Bryden et al. 1991; Macdonald 1998). In a study of the global meridional overturning streamfunctions based on the RAtl and RPac datasets (TRR), an even more robust downwelling feature is apparent at 47°N, which also a feature of Roemmich and McCallister's and Macdonald's calculations.

3) SOUTH ATLANTIC AT 32°S (FIG. 6C AND TABLE 9)

The shallow overturning heat transport of −0.11 PW above 26.2 σ_θ is first removed. There is net downwelling (meridional overturn) north of this section (assumed to be in the northern North Atlantic) into the −17.8 Sv of

TABLE 9. South Atlantic (32°S) zonally averaged overturns.

Layer	Heat transport (PW)	Volume transport (Sv) and temperature transport (PWT)	Heat transport from conversion to NADW (PW)
Total heat transport (Table 1)	0.23	—	—
Shallow overturning (Table 5b)	−0.11	6.2 Sv closed circulation	—
Net intermediate–deep overturning	0.34 PW including Bering Strait	—	—
Surface–26.2 σ_θ (upper thermocline, after shallow overturn subtracted)	—	4.06 Sv 0.27 PWT	0.22
26.2–26.9 σ_θ (lower thermocline)	—	3.34 Sv 0.13 PWT	0.09
26.9–27.4 σ_θ (AAIW)	—	5.15 Sv 0.12 PWT	0.07
27.4 σ_0–45.88 σ_4 (NADW)	—	−17.75 Sv −0.19 PWT	—
Bering Strait	—	−1.35 Sv −0.02 PWT	−0.02
45.88 σ_4–bottom (LCDW/AABW)	—	3.84 Sv 0.02 PWT	−0.03

southward-flowing NADW of 4.1 Sv of the remaining warm surface water (from the Benguela Current), 3.3 Sv of deeper thermocline water, and 5.2 Sv of AAIW. There is also a throughput of −1.35 Sv of Bering Strait water in the NADW layer. The heat transport associated with thermocline to NADW conversion is 0.31 PW, while that associated with AAIW to NADW conversion is only 0.07 PW. The 3.8 Sv of upwelling from the AABW layer into the NADW layer has almost no associated heat transport because of the small temperature change. (This 3.8 Sv is smaller than the 6.7 Sv calculated at 24°N. The difference between the two may be an indicator of the difficulty of estimating near-bottom transport, as described at the start of this section.)

Sensitivity to reducing the Bering Strait throughput to 0.8 or even 0.0 Sv is small (Table 3); the total heat transport changes by only 0.02 PW, as in the North Atlantic where the sensitivity was also small.

The −17.8 Sv of southward flow in the broad NADW layer is comparable to Rintoul's (1991) −17 Sv, Holfort and Siedler's (2001) −21.7 Sv, and Sloyan and Rintoul's (2001a) −20 Sv. The 5.2 Sv of AAIW here compares well with Rintoul's 5 Sv, Holfort and Siedler's 4 Sv (using a smaller density range), and Sloyan and Rintoul's (2001a) 5 Sv. The 3.8 Sv in the AABW layer here is comparable to Rintoul's (1991) 4 Sv, but is likely an underestimate based on neighboring sections in this analysis and compared with Holfort and Siedler's 6.8 Sv. [See comments in section 4b(1) and appendix C.]

4) Indian Ocean at 32°S (Fig. 6d and Table 10)

After the heat transports of the subtropical gyre shallow overturning and the vanishingly small ITF contribution are removed, upwelling is required from the inflowing Circumpolar Deep Water throughout the rest of the water column to balance mass (Toole and Warren 1993; Robbins and Toole 1997). The overturn of 14 Sv reported here is close to the RTInd overturn (nearly the same calculation) and is significantly smaller than the recent Sloyan and Rintoul (2001a) estimate of 23 Sv. As pointed out in RTInd, there is net southward flow in the AAIW layer, due to overcompensation of the northward flow of AAIW by southward-flowing upwelled Circumpolar Deep Water. The heat transport associated with this upwelling is −0.08 PW for upwelling of 10.7 Sv of CDW into the AAIW/IDW layer and −0.16 PW for upwelling of 3.2 Sv of CDW into the thermocline.

Thus the net heating in the Indian Ocean tropical region is balanced by both southward export of heat in the subtropical gyre's shallow overturn and by upwelling from great depth.

5) South Pacific at 28°S (Fig. 6e and Table 11)

After removing the subtropical gyre overturn and the ITF and Bering Strait throughputs (assumed to be in the surface layer), the meridional transports include a remaining southward flow of −4.5 Sv in the EAC's upper layer, and southward flow of −9.3 Sv in the PDW. The bottom waters (Circumpolar Deep Water) flow northward and upwell into the PDW and thermocline waters somewhere north of 28°S. This is similar to the deep Indian Ocean. The 13.8 Sv of northward flow in the deep LCDW layer matches Wunsch et al.'s (1983) estimate but is much lower than Sloyan and Rintoul's (2001a) 26 Sv. As in the Indian Ocean, the deeper AAIW net volume transport at 27.1–27.6 σ_θ is southward, despite the low salinity signature from the south, again because the upwelled CDW converted to PDW extends up to this density range and flows southward. The net heat transport associated with all of the upwelling north of the section is −0.23 PW.

If the ITF and Bering Strait throughput transports extend into the deep ocean [section 4a(5)], the closed cell of deep northern upwelling feeding southward flow out of the Pacific does not extend to the thermocline since the shallow gyre circulation includes all of the southward-flowing EAC. (The deep upwelling to the thermocline instead feeds only the ITF and Bering Strait flows.) The heat transport associated with the deep upwelling is then only −0.13 PW if the ITF/Bering Strait throughput is in the surface layer and 27.1–27.6-σ_θ layer (Table 11), or −0.10 PW if it extends to the bottom (not listed).

6) Southern Ocean overturning south of 30°S (Fig. 7 and Table 12)

What do the three Southern Hemisphere subtropical sections imply for Southern Ocean processes? The isopycnal layers used for the Indian Ocean were used for the composite since the Indian transports could not be easily recalculated.

The total heat transport southward across 30°S is −0.80 PW. The meridional transport in the circumpolar layers (Fig. 7) is remarkably simple, with two main downwelling cells. The upper cell includes a net southward transport of 8 Sv of the warmest water with returning northward transport of waters down to a density of about 27.0 σ_θ. The southward heat transport associated with this upper cell is −0.6 PW. This overturning reflects the formation of Subantarctic Mode Water (SAMW) and possibly AAIW: The maximum net overturning cell may be stronger and reach a little above or below this isopycnal and could easily include the top of the AAIW. Total Ekman volume and temperature transports are small since they are southward in the South Pacific and northward in the Indian and South Atlantic Oceans (Table 1).

The deeper overturning cell consists of net southward transport of all the deep waters from the Northern Hemisphere regions: NADW, PDW, and IDW all downwelling in the Antarctic into the denser Circumpolar Deep Water (CDW) and the northward return transport. The

TABLE 10. Indian Ocean (32°S) zonally averaged overturns for 8 Sv ITF.

Layer	Heat transport (heat flux divergence) (PW)	Volume transport (SV) and temperature transport (PWT)	Heat transport from upwelling (PW)
Total heat transport (Table 1)	−0.59	—	—
Shallow overturning gyre (Table 5a)	−0.27	40.5 Sv closed circulation	—
ITF (Table 6)	−0.07	8 Sv closed circulation	—
Net intermediate and deep overturning	−0.24	—	—
Surface–27.0 γ^n (after shallow overturn subtracted)	—	−3.16 Sv −0.18 PWT	—
27.0–27.12 γ^n (26.89–27.0 σ_θ)	—	−1.54 Sv −0.06 PWT	—
27.12–27.46 γ^n (27.0–27.3 σ_θ) (AAIW)	—	−4.41 Sv −0.01 PWT	—
27.46–27.7 γ^n (27.3 σ_θ–36.65 σ_2) (IDW)	—	−3.53 Sv −0.06 PWT	—
27.7–27.93 γ^n (36.65–36.89 σ_2) (IDW)	—	−1.19 Sv −0.02 PWT	—
27.93–28.11 γ^n (36.89 σ_2–45.88 σ_4) (NADW and CDW)	—	3.97 Sv 0.06 PWT	3.16 Sv −0.16 PW upwell to thermocline
28.11–28.23 γ^n (45.88–46.0 σ_4) (CDW)	—	8.48 Sv 0.03 PWT	and
28.23 γ^n–bottom (46.0 σ_4–bottom) (CDW)	—	1.39 Sv 0.002 PWT	10.67 Sv −0.08 PW upwell to IDW/AAIW

northward transport is 22.0 Sv below 45.88 σ_4 (28.11 γ^n), where σ_4 is potential density relative to 4000 dbar and γ^n is neutral density. This is comparable to Schmitz's (1995) global summary based on many regional analyses, although the northward CDW in the Pacific is weaker here (13 vs 20 Sv in Schmitz). It is also comparable to Ganachaud and Wunsch's (2000) Southern Ocean overturn of 21 ± 6 Sv, but is much smaller than Sloyan and Rintoul's (2001a) 54 Sv, which was constrained by air–sea heat flux estimates south of 30°S. The southward heat transport associated with LCDW overturn is −0.14 PW (heat lost by the ocean in the Southern Ocean). Again the heat transport is robust, but the overturning strength is likely an underestimate because of the coarse layer resolution. For instance, on the South Pacific section, the bottommost two CDW layers (Table 11, Fig. 7) carry 9.98 Sv northward below 37.05 σ_2, where σ_2 is potential density relative to 2000 dbar. However, the top of these layers includes southward flow. When finer layers are used, a northward transport of 13.66 Sv below 45.84 σ_4 is found. For the South Atlantic section, finer layer divisions produce 3.77 Sv northward below 45.86 σ_4 as opposed to the 1.96 Sv used here since some southward NADW is included in the coarse layers here. Thus the net deep water overturn might be 5–6 Sv larger than 22 Sv. Comparison and interpretation of this overturn relative to recent AABW production estimates, for instance, Orsi et al.'s (1999) estimate of 8–9 Sv at densities greater than 28.27 γ^n, are considered in a separate study (TRR).

The heat transport of −0.80 PW is divided into 0.23 and −1.02 PW for the Atlantic and Indian/Pacific Oceans. This is comparable to Macdonald's (1993) −0.7 PW across 30°S, divided into 0.3 and −1.0 PW in the Atlantic and Indian/Pacific Oceans. The total compares less well with Wijffels et al.'s (2001) recent circumpolar estimate of −0.46 PW, divided into 0.4 and −0.9 PW in the Atlantic and Indian/Pacific Oceans, possibly because the exact section latitudes matter. That is, in the Pacific, the heat divergence between 28° and 43°S calculated here is large. Since Wijffels et al. used the WOCE 32°S section, their heat transport may differ considerably from that at either 28° or 43°S.

5. Discussion

The meridional heat transport associated with the local shallow overturning subtropical gyre in each ocean is poleward. The heat loss poleward of and heat gain equatorward of the subtropical sections is associated with the upper ocean's subduction process (Luyten et al. 1983). This includes poleward advection of warm water by the major western boundary currents, cooling, and subduction of the equatorward flow. Heat gain in lower latitudes completes the circuit, although the pathways of this required upwelling have not been diagnosed.

The subtropical gyre overturning heat transports in the Northern Hemisphere are larger than those of the Southern Hemisphere (0.4 to 0.6 PW vs −0.1 to −0.3 PW). This is reflected in climatological ocean–atmosphere heat flux maps (NCEP in Fig. 1; Hsiung 1985; Barnier et al. 1994; Keith 1995), where the Gulf Stream and Kuroshio surface heat losses are stronger than those in the Brazil, East Australia, and Agulhas Currents.

In the shallow overturning heat transport calculation,

TABLE 11. South Pacific (28°S) zonally averaged overturns for 8 Sv ITF and 1.35 Sv Bering Strait.

	ITF/BS in upper layer only		ITF/BS distributed in depth	
Layer	Heat transport (PW) or temperature transport (PWT) and volume transport (Sv)	Heat transport from conversion to PDW (PW)	Heat transport (PW) or temperature transport (PWT) and volume transport (Sv)	Heat transport from conversion to PDW (PW)
Total heat transport (Table 1)	−0.03 PWT −0.40 PWT* = −0.43 PW	—	−0.03 PWT −0.40 PWT* = −0.43 PW	—
Shallow overturning gyre (Table 5a)	−0.38 PW 19.5 Sv closed circulation	—	−0.26 PW 28.4 Sv closed circulation	—
ITF (Tables 5a and 6)	0.46 PWT −0.4 PWT* = 0.06 PW 8 Sv closed circulation	—	0.33 PWT −0.40 PWT* = −0.07 PW 8 Sv closed circulation	—
Bering Strait (Table 6)	0.08 PW 1.35 Sv closed circulation	—	0.03 PW 1.35 Sv closed circulation	—
Net intermediate and deep overturning	−0.19 PW	—	−0.13 PW	—
Surface–27.1 σ_θ (thermocline and ITF/BS throughputs, after shallow overturn subtracted)	−4.51 Sv −0.14 PWT	—	—	—
27.1–27.6 σ_θ (AAIW or PDW1)	−2.87 Sv −0.06 PWT	—	−7.40 Sv −0.13 PWT	—
27.6 σ_θ–36.96 σ_2 (PDW2)	−5.37 Sv −0.04 PWT	—	−5.37 Sv −0.04 PWT	—
36.96 σ_2–45.84 σ_4 (PDW3)	−1.01 Sv −0.006 PWT	—	−1.01 Sv −0.006 PWT	—
45.84–45.88 σ_4 (LCDW1)	3.39 Sv 0.02 PWT	4.51 Sv/−0.12 PW to thermocline and 9.25 Sv/−0.07 PW to PDW	3.39 Sv 0.02 PWT	None to thermocline and AAIW except to feed ITF/BS and 9.25 Sv/−0.13 PW to PDW
45.88–45.92 σ_4 (LCDW2)	1.59 Sv 0.01 PWT		1.59 Sv 0.01 PWT	
45.92 σ_4–bottom (LCDW3)	8.78 Sv 0.03 PWT		8.78 Sv 0.03 PWT	

* ITF temperature transport.

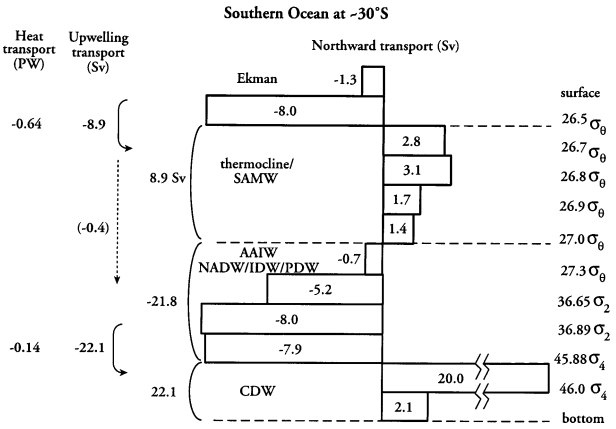

FIG. 7. Global (sum of Pacific, Atlantic, Indian Ocean) meridional overturning transport across 30°S (Table 12). Layers used are those of the Indian Ocean 32°S section (Fig. 6d).

upwelling from below the maximum subduction density was neglected. Ekman suction occurs poleward of the subtropical gyres, and some of the upwelled water feeds the surface layer of the subtropical gyre through equatorward Ekman transport across the gyre boundary—across the subantarctic front in the Southern Ocean or the subpolar fronts in the Northern Hemisphere. If included in the shallow gyre overturning heat transport, the upwelling would reduce the poleward heat transports. On the other hand, the overturns south of 30°S (Table 12) show no net southern upwelling from the AAIW layer into the thermocline, nor is there evidence of net upwelling from below the maximum subduction density in the North Pacific and North Atlantic budgets (Tables 7 and 8).

The Indonesian Throughflow was assumed here to impact the shallow subducted layers in both the Indian and Pacific Oceans. The RTInd and RPac analyses have more than enough warm water transport in the Agulhas and in the eastern subtropical South Pacific to accommodate the ITF. The ITF is only slightly different in

TABLE 12. Southern Ocean (~30°S) zonally averaged overturns; total layer transports with no shallow overturn adjustments. Atlantic, Pacific, and Indian Ocean combined, assuming 8 Sv ITF and 1.35 Bering Strait (see text). Total heat transport: −0.80 PW.

Layer	Individual ocean transports (Sv) A = Atlantic I = Indian P = Pacific	Volume transport (Sv) and temperature transport (PWT)	Heat transport from downwelling (PW)
Ekman layer	0.99 (A) 2.17 (I) −4.41 (P)	−1.26 Sv −0.17 PWT	−0.64 downwelling to thermocline and SAMW and
Surface–26.55 γ^n (Surface–26.5 σ_θ)	1.88 (A) −15.31 (I) 5.43 (P)	−8.00 SV −0.86 PWT	−0.04 downwelling to LCDW (ignore)
26.55–26.78 γ^n (26.5–26.7 σ_θ)	1.61 (A) 0.54 (I) 0.67 (P)	2.82 Sv 0.15 PWT	—
26.78–26.90 γ^n (26.7–26.81 σ_θ)	1.72 (A) 1.15 (I) 0.23 (P)	3.10 Sv 0.13 PWT	—
26.90–27.0 γ^n (26.8–26.89 σ_θ)	1.08 (A) 0.30 (I) 0.30 (P)	1.68 Sv 0.05 PWT	—
27.0–27.12 γ^n (26.89–27.0 σ_θ)	1.31 (A) −1.54 (I) 1.65 (P)	1.43 Sv 0.03 PWT	—
27.12–27.46 γ^n (27.0–27.3 σ_θ) (AAIW)	3.23 (A) −4.41 (I) 0.52 (P)	−0.66 Sv 0.06 PWT	−0.14 downwelling to CDW layers
27.46–27.7 γ^n (27.3 σ_θ–36.65 σ_2)	0.17 (A) −3.53 (I) −1.81 (P)	−5.17 Sv −0.09 PWT	
27.7–27.93 γ^n (36.65–36.89 σ_2)	−3.51 (A) −1.19 (I) −3.35 (P)	−8.04 Sv −0.09 PWT	
27.93–28.11 γ^n (36.89 σ_2–45.88 σ_4)	−11.93 (A) 3.97 (I) 0.07 (P)	−7.89 Sv −0.08 PWT	
28.11–28.23 γ^n (45.88–46.0 σ_4) (LCDW)	1.43 (A) 8.48 (I) 10.05 (P)	19.96 Sv 0.06 PWT	—
28.23 γ^n–bottom (46.0 σ_4–bottom) (LCDW)	0.66 (A) 1.39 (I) 0.0 (P)	2.05 Sv 0.003 PWT	—

temperature than the assumed Indian (Agulhas) outflow and South Pacific inflow (if above the thermocline), and so the heat transport associated with the ITF is small and the sign indeterminate. If the Pacific inflow feeding the ITF originates below the surface layer, hence colder than estimated here, then the ITF loop is associated with net surface heat gain in the Pacific. If the Indian outflow of the ITF were deeper in the Agulhas than assumed here, then its transit through the Indian Ocean would be associated with net heat loss, which seems unlikely.

Heat transports associated with deepwater formation and Northern Hemisphere intermediate water formation are closely tied to the direction and strength of the overturning circulations in each ocean. The Pacific overturn is weak, and hence the North Pacific meridional heat transport is dominated by shallow gyre overturn. The North Atlantic overturn is strong, and so the North Atlantic meridional heat transport is dominated by LSW and NADW formation. This domination has long been understood to extend to the South Atlantic. The deep South Pacific overturning heat transport of −0.1 to −0.2 PW is associated with upwelling and is the same order of magnitude as the shallow overturning heat transport of −0.2 to −0.3 PW. Likewise in the Indian Ocean, deep upwelling north of 32°S provides a substantial poleward heat transport of −0.2 PW, of the same order of magnitude as the shallow overturning heat transport of −0.3 PW.

6. Summary

1) The processes associated with subtropical subduction transport heat poleward. This is apparent even in the Southern Hemisphere once the complicating deep overturning cells and Indonesian Throughflow are removed. Regardless of the strength or even presence of intermediate/deep overturn, midlatitude heat loss would continue to be associated with poleward heat transport; that is, in a climate scenario with a weakened or absent meridional overturning circulation, there would still be major poleward heat transport, like that of the North Pacific in today's climate.
2) Heat transport in the North Pacific, unlike that of all other oceans, is dominated by shallow processes, made even shallower in physical space by the strong stratification of the North Pacific.
3) Much of the North Atlantic heat transport is associated with intermediate and deep overturn, but a shallow gyre component is nevertheless present, associated with the large ocean heat loss in the Gulf Stream.
4) The Indonesian Throughflow has only a small effect on the heat budget of the Indian Ocean, given recent observations of ITF temperature transport (Vranes et al. 2002), and assuming that the associated outflow in the subtropical Indian Ocean is in the upper ocean, as seems reasonable. This small impact of the ITF extends to the Pacific if the source waters of the ITF flowing northward in the South Pacific are above the thermocline, yielding a net associated heat loss in the Pacific. However, if the ITF source waters at 28°S are deeper, as is possible, there is an associated heat gain in the Pacific. This volatility in the estimated impact of the ITF indicates the importance of continuing to evaluate the complete ITF loop, its source and sink waters and passage through the archipelago.
5) Upwelling from the deep waters to the upper ocean is an important component of the heat budget in the Indian and South Pacific Oceans. The major contrast between the South Atlantic's deep overturning heat transport and that of the Indian and South Pacific Oceans is that the latter two involve deep upwelling north of the zonal sections, while the South Atlantic involves NADW formation (downwelling).
6) Downwelling (water mass formation) in the Antarctic is split into two overlying cells: transformation of thermocline waters to SAMW/AAIW in the upper ocean, and transformation of northern source deep waters into bottom waters. These cells carry a significant amount of heat; that is, the heat transport associated with upwelling in the Indian and Pacific is not solely due to NADW formation, but also includes the Southern Ocean component.

This analysis indicates that, alone of all the oceans, the North Pacific can be successfully monitored with partial water column measurements. This is being done, for example, by Roemmich et al. (2001) using repeat partial-depth XBT sections, since deep water processes do not carry much heat there. The North Atlantic especially requires monitoring to the bottom, since the important LSW/NADW overturning components are close to their time-varying and volumetrically large sources. The Indonesian throughflow may be a critical part of the global heat budget, in the same way that Ekman temperature transports are critical, since both are confined to warm waters.

The purpose of this exercise was to assess the strength of various specific processes in carrying heat. There were many simplifications. Extensions should be made to other processes. Examples include upwelling associated with equatorward subpolar–subtropical cross-gyre transport at the sea surface, and tropical overturning cells. Within the ocean's intermediate and deep isopycnal layers there are major opposing meridional volume transports leading to relatively minor net meridional transport. While these opposing transports may have little effect on heat transport since the temperature differences between northward and southward flows within isopycnal layers are small, they could have a larger impact on freshwater, nutrient, and carbon transports.

Acknowledgments. Tremendous gratitude is expressed to J. Reid, S. Anderson, and P. Robbins for the geostrophic velocity analyses, and to P. Robbins, H. Bryden, J. Toole, and two anonymous, thorough reviewers for their comments on the manuscript. The original heat transport calculations were created for an American Geophysical Union Chapman conference in June 1998. Support was from the National Science Foundation funding for the World Ocean Circulation Experiment, through Grants OCE-9712209 and OCE-9529584.

APPENDIX A

Comparison with the Bryan–Bryden Decomposition

Following a number of earlier studies, notably Bryan (1982) and Bryden (1993), and calculations influenced by Bryden (Wijffels et al. 1996; Robbins and Toole 1997), Bryden and Imawaki (2001) summarized a division of heat transports into three mass-conserving elements: 1) barotropic (''leakage''), 2) baroclinic, and 3) horizontal/eddy. They identified the horizontal component with the horizontal, wind-driven gyre circulation and the baroclinic component with the deeper overturn. The barotropic component is due to net mass flux through a given zonal section, balanced by the Bering Strait and/or Indonesian Throughflow as appropriate. These three components are philosophically similar to the 1) Bering Strait/Indonesian Throughflow components, 2) intermediate/deep overturn, and 3) shallow overturn calculated here. Similar components were used

TABLE A1. Subtropical section heat transports with Bryan (1982)/Bryden and Imawaki (2001) decomposition.

Section	Total heat transport (PW) (Tables 1 and 6)	Decomposition used here			Bryden and Imawaki (2001) decomposition		
		Throughput heat transport (PW) (ITF/Bering) (Table 6)	Shallow gyre heat transport (PW) (Tables 4 and 5)	Intermediate/ deep overturn heat transport (PW)	Barotropic (''leakage'') heat transport (PW)	Horizontal gyre and eddy heat transport (PW)	Baroclinic heat transport (PW)
Atlantic 24°N	1.28 PW	−0.02 PW	0.40	0.88	−0.04 PW	0.12	1.20
Pacific 24°N	0.81 PW	0.14 PW	0.57	0.27	0.03 PW	0.49	0.30
Atlantic 32°S	0.23 PW	−0.02 PW	−0.11	0.34	−0.03 PW	−0.27	0.55
Pacific 28°S assuming 8 Sv ITF and 1.35 Bering	−0.03 PWT − 0.40 PWT* = −0.43 PW	0.46 PWT − 0.40 PWT* = 0.06 PW	−0.24	−0.24	0.17 PWT − 0.40 PWT* = −0.23 PW	−0.16	−0.05
Indian 32°S	−0.99 PW + 0.40 PW* = −0.59 PW	−0.47 PWT + 0.40 PWT* = −0.07 PW	−0.27	−0.24	**0.18 PW	**−0.19	**−0.41

* Temperature transport for meridional flow through the section, associated with the ITF and Bering Strait, minus the temperature transport for the ITF itself.
** Values from Robbins and Toole (1997), their Table 5, with silica constraints. Indian Ocean section values in the present work, provided by Robbins, include both the silica constraint and one for LADCP-observed velocities in the Agulhas, and so the total heat transports are not equal.

in RTInd (values shown in Table A1, using isopycnal layers and with the ITF in the uppermost layer rather than strictly following the Bryden and Imawaki formulation) and also in Bryden and Beal (2001).

The advantage of the Bryan (1982) and Bryden and Imawaki (2001) decomposition is that it requires neither a choice of isopycnal layers, nor, as required for the shallow overturning transport used here, a choice for the maximum subtropical subduction density. Thus it is a useful diagnostic in numerical model calculations in which the correspondence of densities and processes with those of the actual ocean are likely inexact. The disadvantage of the shallow overturn decomposition is that it is not useful outside the subducting subtropical gyres. Other decompositions might be developed that would capture the heat transport associated with other specific mass-conserving parts of the intermediate/deep overturn.

Because of the increasing use and practicality of the Bryan–Bryden components, the latter quantities were computed to compare with the three components used here (Table A1). It is apparent that the shallow overturning and horizontal gyre heat transports are not directly equivalent, nor are the other two pairs of quantities (intermediate/deep and baroclinic; ITF/Bering Strait and barotropic). This is because the horizontal gyre transport includes horizontal (with depth) temperature differences at all depths and does not include Ekman transport, whereas the shallow overturn includes Ekman transport and only the contrasts in temperature shallower than the maximum subduction density. Likewise, the baroclinic heat transport includes the Ekman transport and any possible parts of the shallow overturn that express themselves at different depths. And finally, the ITF/Bering Strait heat transports here involve only the part of the flow that is assumed to feed these straits, whereas the barotropic component is the section-averaged velocity and temperature. (The Ekman transport effect is most apparent for the North Pacific section with its large Ekman volume transport and relatively strong shallow overturn.)

APPENDIX B

Ekman Transport Sensitivity to Wind Products

Ekman transports were calculated using annual average wind stresses from Hellerman and Rosenstein (1983, hereafter HR). Numerous comparisons of this wind product with more recent products reveal regional differences. Harrison's (1989) list of Ekman transports based on HR and his own climatology is the basis for the last two columns of Table B1, showing the HR transports about 20% larger. Harrison's HR values differ from those here (Table B1), presumably because the latter were interpolated to every station pair, and the sections were not exactly zonal. Holfort and Siedler (2001) compared Ekman transport from HR winds and the South-

TABLE B1. Ekman volume transports (Sv) and associated temperature and heat transports.

Section	HR Ekman volume and temperature transport (Sv and PWT) (Table 1)	Total heat transport with HR (PW) (Table 1)	NCEP Ekman volume and temperature transport (Sv and PWT)	Total heat transport with NCEP (PW)	Macdonald (1998) ECMWF Ekman volume transport (Sv)	Harrison (1989) HR Ekman transport (Sv)	Harrison (1989) Ekman transport (Sv)
Atlantic 59°N	−1.2 Sv −0.04 PWT	0.70	−1.3 Sv −0.04 PWT	0.69	—	−1.7	−1.4
Atlantic 53°N	−2.6 Sv −0.10 PWT	0.62	−2.2 Sv −0.09 PWT	0.68	—	−3.1	−2.6
Atlantic 45°N	−2.9 Sv −0.16 PWT	0.62	−2.4 Sv −0.14 PWT	0.62	−3.8 (48°N)	−4.1	−3.4
Atlantic 36°N	−3.4 Sv −0.28 PWT	0.86	−2.3 Sv −0.20 PWT	0.92	−2.7	−3.5	−3.3
Atlantic 32°N	−1.5 Sv −0.14 PWT	−0.01[a]	−0.8 Sv −0.08 PWT	0.03[b]	—	−1.3	−1.4
Atlantic 24°N	5.9 Sv 0.56 PWT	1.28	4.8 Sv 0.46 PWT	1.20	5.4	7.4	5.6
Atlantic 8°N	10.7 Sv 1.13 PWT	0.73	10.2 Sv 1.09 PWT	0.70	9.3 (11°N)	11.4	8.7
Atlantic 8°S	−12.8 Sv −1.32 PWT	−0.22[a]	−12.0 Sv −1.23 PWT	−0.15[b]	—	−14.0	−11.2
Atlantic 11°S	−11.6 Sv −1.17 PWT	−0.38[a]	−10.7 Sv −1.08 PWT	−0.31[b]	−11.2	−12.5	−9.9
Atlantic 16°S	−8.6 Sv −0.82 PWT	0.61	−7.8 Sv −0.75 PWT	0.68	—	−8.9	−7.3
Atlantic 24°S	−3.8 Sv −0.32 PWT	0.37	−3.3 Sv −0.29 PWT	0.45	−4.3	−4.4	−3.3
Atlantic 32°S	1.0 Sv 0.08 PWT	0.23	1.2 Sv 0.09 PWT	0.24	0.2	1.2	1.8
Atlantic 40°S	7.2 Sv 0.32 PWT	−0.03	7.0 Sv 0.31 PWT	−0.04	—	—	—
Pacific 47°N	−5.2 Sv −0.17 PWT	0.01	−4.3 Sv −0.17 PWT	0.04	−5.4	−5.5	−4.2
Pacific 35°N	−4.3 Sv −0.32 PWT	0.77	−4.1 Sv −0.31 PWT	0.78	—	−4.9	−4.5
Pacific 24°N	11.3 Sv 1.07 PWT	0.81	8.6 Sv 0.82 PWT	0.60	8.8	12.7	9.2
Pacific 10°N	39.6 Sv 4.28 PWT	1.25	29.6 Sv 3.24 PWT	0.36	24.3 (W38.6 Sv)[c]	41.7	31.6
Pacific 28°S[b]	−4.4 Sv −0.38 PWT	−0.03 − 0.40[b] = −0.43	−3.2 Sv −0.28 PWT	0.08 − 0.40[b] = −0.32	−5.5	−4.9	−5.3
Pacific 43°S[b]	7.8 Sv 0.39 PWT	0.45 − 0.40[b] = 0.05	7.7 Sv 0.39 PWT	0.44 − 0.40[b] = 0.04	9.8	7.9	0.5
Indian 32°S[b]	2.2 Sv 0.13 PWT	−0.99 + 0.40[b] = −0.59	0.8 Sv 0.6 PWT	—	0.5	1.3	0.8

[a] Serious problems are inferred for the geostrophic portion of these total heat transport estimates.
[b] Vranes et al. (2002) temperature transport for ITF.
[c] Pacific 10°N: W38.6 Sv is Wijffels et al. (1996) estimate based on a constrained inverse model, starting with an initial estimate of 37 Sv.

ampton climatology for their South Atlantic sections and found the HR winds stronger than Southampton Oceanography Centre (SOC) by about 20%. ECMWF Ekman transports from Macdonald (1998) at sections that match those used here are also listed in Table B1; most are smaller than the HR Ekman transports.

The NCEP reanalysis online long-term monthly mean surface momentum flux was used to compute the annual average Ekman transport for each station pair and summed for the sections (Table B1), to compare with the HR Ekman transports. Temperature transports were calculated with Levitus and Boyer (1994) 30-m mean temperatures. The geostrophic transports for the Pacific and Atlantic sections were then recomputed, adjusting to the NCEP Ekman transports. The heat transport elements and totals are listed in Table B1.

Overall the HR Ekman transport magnitudes are larger than the NCEP magnitudes (18 out of 20 sections), as reported by others. The mean difference was 16%, with large fluctuations. These differences occur in all regions. Heat transport adjustments are consistent with the decreased Ekman transport for the NCEP winds: less southward heat transport in the Northern Hemisphere westerlies and Southern Hemisphere trades and vice versa. The only exception is in the South Atlantic westerlies (32° and 40°S), where the NCEP and HR Ekman transports are nearly the same size. The mean difference in heat transports in all westerly wind regions is 0.03 PW, which is negligible. The mean change in heat transport in the Southern Hemisphere trade wind regions is 0.08 PW, which is still within the other errors. However, the change in heat transport in the North Pacific trade wind region is large: the NCEP winds result in northward heat transports that are lower by 0.21 PW at 24°N and 0.89 PW at 10°N. These are unacceptably large. The HR Ekman transports are retained in this manuscript for continuity with previous heat transport calculations. However, the NCEP-based transports will be used in future work with these transport fields.

As an abbreviated test of the ECMWF winds, I adopted Macdonald's (1998) ECMWF-based 24.6 Sv Ekman transport for 10°N in the Pacific. The total heat transport at this latitude is strongly affected by the large Ekman transport, and the much smaller ECMWF transport led to a southward total heat transport, which is inconsistent with previous results including those based on air–sea fluxes. Macdonald also found the 24.6 Sv to be too weak, and therefore used Wijffel's et al.'s (1996) larger 38.6 Sv, which was derived from HR winds subjected to inverse model constraints.

APPENDIX C

Data Diagnostics

The hydrographic sections in RAtl and RPac were assembled from many different datasets (tables in RAtl and RPac; Tables 1 and C1 here), most from the International Geophysical Year (IGY) program of the late 1950s, long lines in the 1960s, and densely sampled long lines in the 1980s, with additional individual stations from other datasets to fill gaps. Station spacing, vertical sample spacing, and the depth above the bottom (DAB) of the deepest sample on each profile vary widely. Discretely sampled hydrographic data were used by RAtl and RPac for almost all sections even when CTD data were available; subsampled CTD data were used for 10°N in the Pacific. Prior to their use in RAtl and RPac, the temperature and salinities were subjected to rigorous quality control by A. Mantyla, and some but not all large vertical sampling gaps were filled by interpolation.

The meridional heat transport estimates at 32°N, 8°S, and 11°S (and marginally 40°S) in the Atlantic (section 3) differ greatly from those at adjacent latitudes and from previous analyses of Atlantic heat transports (references in text). This suggests that the geostrophic reference velocities for these sections were of lower quality than for other sections and that heat transport error might vary significantly among the other sections. Sampling diagnostics (Table A3) include station spacing, vertical bottle spacing, DAB, and percentages of stations with large vertical sampling gaps and large DAB. The mean and maximum adjustments to station pair transports to match Reid's station pair transports were also tabulated. The station pair transports computed here differed from Reid's because of the vertical interpolation methods (matched parabolas in RAtl/RPac and an Akima cubic spline in my processing.) The adjustments were slight where vertical sample coverage was good, but were large ($>$13 Sv per station pair) when vertical sampling gaps were greater than 800 m in the thermocline. The uniform velocity adjustments applied to the geostrophic velocities to balance the Ekman transport are also listed, but do not appear to be related to failure of the heat transport calculations.

From Table C1, the best predictors of poor performance are inhomogeneous data sources and large vertical sampling gaps. The Atlantic 32°N and 40°S sections include many separate datasets (five and eight, respectively), many from the IGY and some dating back to the Meteor expedition in 1925. By this criterion, the Pacific 35°N section might also be problematic; its reasonable heat transport estimate might reflect the strength of the shallow overturn in this gyre and hence importance of the upper gyre circulation and Ekman transport. Net property transports are likely sensitive to use of multiple cruises because individual station pair transports, which are often comparable in size to the net transport, are due to synoptic eddy and current activity that varies over weeks and are then aliased into the net transport if the section is not synoptic.

The Atlantic 8° and 11°S sections are each based on single datasets, from the IGY and from 1983, respectively. The latter dataset is well sampled in the horizontal and vertical, especially with regard to CTD data,

TABLE C1. Section diagnostics.

Section	No. of separate cruises	No. of stations	Mean (max) station spacing (km)	Ekman velocity adjustment ($\times 10^{-4}$ cm s^{-1})	Mean station pair transport adjustment to match Reid (Sv)	Max station pair transport adjustment to match Reid (Sv)	No. and (%) of stations with vertical gap >500 m	Mean (min) depth of vertical gaps >500 m	No. and (%) stations with depth above bottom > 200 m
Atlantic 59°N	1	55	58 (83)	1.88	0.2	1.6	1 (1.8%)	1023	—
Atlantic 53°N	1	44	66 (119)	3.75	0.1	1.0	1 (2.3%)	989	—
Atlantic 45°N	1	40	77 (142)	2.71	0.1	0.5	2 (5.0%)	2743 (1906)	3 (7.5%)
Atlantic 36°N	1	101	56 (116)	1.44	0.2	0.7	0	—	1 (1.0%)
Atlantic 32°N	5	47	134 (221)	0.60	0.4	2.5	8 (17.0%)	3831 (1833)	1 (2.1%)
Atlantic 24°N	1	97	64 (124)	−1.89	0.1	0.7	0	—	1 (1.0%)
Atlantic 8°N	1	31	159 (197)	−5.86	0.7	2.0	1 (4.8%)	3225	9 (29.0%)
Atlantic 8°S	1	30	180 (391)	6.11	1.8	11.5	2 (6.7%)	3423 (3350)	7 (23.3%)
Atlantic 11°S	1	66	83 (186)	4.91	1.3	20.0	8 (12.1%)	4026 (2043)	2 (3.0%)
Atlantic 16°S	1	33	166 (193)	4.11	0.5	2.8	2 (6.1%)	3896 (3133)	10 (30.3%)
Atlantic 24°S	2	46	130 (282)	1.66	0.2	1.0	0	—	7 (15.2%)
Atlantic 32°S	1	41	173 (453)	−0.46	0.3	2.5	2 (4.9%)	3281 (2601)	7 (17.1%)
Atlantic 40°S	7	42	191 (1614)	−2.39	0.1	0.6	4 (9.5%)	3149 (1324)	4 (9.5%)
Pacific 47°N*	1	115	65 (91)	1.43	0.5 (0.1)	23.3 (0.8)	13 (11.3%)	3716 (1392)	5 (4.3%)
Pacific 35°N	8	72	129 (361)	0.97	0.3	4.5	8 (11.1%)	3641 (1526)	9 (12.5%)
Pacific 24°N*	1	202	62 (157)	−1.99	0.7 (0.1)	24.0 (0.7)	4 (2.0%)	3660 (1497)	4 (2.0%)
Pacific 10°N	1	207	78 (183)	−5.59	0.2	1.1	0	—	7 (3.4%)
Pacific 28°S	1	49**	265 (603)	0.93	0.5	3.1	0	—	3 (6.1%)
Pacific 43°S	1	42**	257 (1120)	−2.04	0.3	2.0	1 (2.4%)	2890	5 (11.9%)
Indian 32°S	1	106	78 (185)	—	—	—	12 (11.3%)	2729 (992)	2 (1.9%)

* Pacific 24° and 47°N: The first number listed for transport adjustments to match RAtl and RPac (columns 6 and 7) includes all stations. At 47°N, one station (26) created the high maximum station pair adjustment. At 24°N, three stations (349 353, 357) produced the large maximum adjustment. All of these stations had very large (>1000 m) sampling gaps in the thermocline. The adjustment ranges excluding these stations are listed in parentheses.

** Pacific 28° and 43°S: many stations from these Scorpio expedition cruises were not included in RPac and hence are not included here.

but bottle sampling had very large gaps in the deep water in the western basin, where the Antarctic Bottom Water flows north. Since RAtl used the gappy bottle data, the AABW flow estimate is suspect and is indeed very large, balancing most of the southward NADW flow whereas much of this northward flow should be in the thermocline and above. The 8°S section also has several stations with large vertical gaps near the western boundary. Possibly because these sections are adjacent, RAtl chose reference velocities that created a continuous and strong northward AABW flow on the two sections. The 8°N and 16°S sections, in contrast, have almost no northward near-bottom flow in RAtl, but also are very poorly sampled near the bottom.

Vertical sampling gaps lead to error because the data must be interpolated and this error is most problematic when the gaps are in important vertical gradients or in layers that are involved in the net transports; in the Atlantic this is throughout the water column. The missing data in midwater column at 8°S led to interpolated profiles that differed unphysically from adjacent well-sampled profiles.

Other large sampling gaps are in the Pacific, where the greater ocean depth resulted in reduced vertical coverage. RAtl/RPac excluded most 28° and 43°S stations with large vertical sampling gaps, thus reducing the horizontal resolution, but retained all stations on the North Pacific sections, leading to some error in vertical interpolation. This was reflected in large station transport adjustments when sampling gaps were in the thermocline, but not when they were in the abyssal waters with much lower vertical gradients. Large heat transport errors from this source are not apparent in the Pacific presumably because the main contribution to heat transport is in the upper ocean circulation.

The main conclusions from these diagnostics are the obvious ones that informed the WOCE Hydrographic Programme planning: that synoptic datasets are preferred and that vertical sampling must be adequate to capture the vertical gradients and layers that impact transports. CTD data are preferable for mass, heat, and freshwater transports but of course cannot be used for other properties. Deficiencies in DAB impact heat transports here only if the net volume transports are not balanced in the proper part of the water column. However, large DABs likely have a major impact on the overturning streamfunction (TRR) and property transports where abyssal waters are important in the budgets.

REFERENCES

Baringer, M. O., and R. Molinari, 1999: Atlantic Ocean baroclinic heat flux at 24 to 26°N. *Geophys. Res. Lett.,* **26,** 353–356.

Barnier, B., L. Siefridt, and P. Marchesiello, 1994: Thermal forcing for a global ocean circulation model using a three-year climatology of ECMWF analyses. *J. Mar. Syst.,* **6,** 363–380.

Beal, L. M., and H. L. Bryden, 1999: The velocity and vorticity structure of the Agulhas Current at 32S. *J. Geophys. Res.,* **104,** 5151–5176.

Broecker, W. S., 1991: The great ocean conveyor. *Oceanography,* **4,** 79–89.

Bryan, K., 1982: Seasonal variation in meridional overturning and poleward heat transport in the Atlantic and Pacific Oceans: A model study. *J. Mar. Res.,* **40,** 39–53.

Bryden, H. L., 1993: Ocean heat transport across 24 latitude. *Interactions Between Global Climate Subsystems: The Legacy of Hann, Geophys. Monogr.,* Vol. 75, Amer. Geophys. Union, 65–75.

——, and L. M. Beal, 2001: Role of the Agulhas Current in Indian Ocean circulation and associated heat and freshwater fluxes. *Deep-Sea Res.,* **38,** 1821–1845.

——, and S. Imawaki, 2001: Ocean heat transport. *Ocean Circulation and Climate,* G. Siedler, J. Church, and J. Gould, Eds., Academic Press, 455–474.

——, D. H. Roemmich, and J. A. Church, 1991: Ocean heat transport across 24-degrees-N in the Pacific. *Deep-Sea Res.,* **38,** 297–324.

Chong, J. C., J. Sprintall, S. Hautala, W. L. Morawitz, N. A. Bray, and W. Pandoe, 2000: Shallow throughflow variability in the outflow straits of Indonesia. *Geophys. Res. Lett.,* **27,** 125–128.

Friedrichs, M. A. M., and M. M. Hall, 1993: Deep circulation in the tropical North Atlantic. *J. Mar. Res.,* **51,** 697–736.

Ganachaud, A., and C. Wunsch, 2000: Improved estimates of global ocean circulation, heat transport and mixing from hydrographic data. *Nature,* **408,** 453–456.

——, C. Wunsch, J. Marotzke, and J. Toole, 2000: Meridional overturning and large-scale circulation of the Indian Ocean. *J. Geophys. Res.,* **105,** 26 117–26 134.

Gordon, A. L., 1986: Interocean exchange of thermocline water. *J. Geophys. Res.,* **91,** 5037–5046.

——, S. B. Ma, D. B. Olson, P. Hacker, L. D. Talley, A. Ffield, and D. Wilson, 1997: Advection and diffusion of Indonesian throughflow water within the Indian Ocean south equatorial current. *Geophys. Res. Lett.,* **24,** 2801–2804.

——, R. D. Susanto, and A. L. Ffield, 1999: Throughflow within Makassar Strait. *Geophys. Res. Lett.,* **26,** 3325–3328.

Hall, M. M., and H. L. Bryden, 1982: Direct estimates and mechanisms of ocean heat transport. *Deep-Sea Res.,* **29,** 339–359.

Harrison, D. E., 1989: On climatological monthly mean wind stress and wind stress curl fields over the World Ocean. *J. Climate,* **2,** 57–70.

Hellerman, S., and M. Rosenstein, 1983: Normal monthly wind stress over the world ocean with error estimates. *J. Phys. Oceanogr.,* **13,** 1093–1104.

Holfort, J., and G. Siedler, 2001: The meridional oceanic transports of heat and nutrients in the South Atlantic. *J. Phys. Oceanogr.,* **31,** 5–29.

Hsiung, J., 1985: Estimates of global oceanic meridional heat transport. *J. Phys. Oceanogr.,* **15,** 1405–1413.

Jayne, S. R., and J. Marotzke, 2001: The dynamics of ocean heat transport variability. *Rev. Geophys.,* **39,** 385–412.

Keith, D. W., 1995: Meridional energy transport: Uncertainty in zonal means. *Tellus,* **47A,** 30–44.

Koltermann, K. P., A. V. Sokov, V. P. Tereschenkov, S. A. Dobroliubov, K. Lorbacher, and A. Sy, 1999: Decadal changes in the thermohaline circulation of the North Atlantic. *Deep-Sea Res.,* **46,** 109–138.

Lavin, A., H. L. Bryden, and G. Parilla, 1998: Meridional transport and heat flux variations in the subtropical North Atlantic. *Global Atmos. Ocean Syst.,* **6,** 231–241.

Levitus, S., and T. Boyer, 1994: Temperature. Vol. 4, *World Ocean Atlas 1994,* NOAA Atlas NESDIS 4, 117 pp.

Luyten, J. L., J. Pedlosky, and H. Stommel, 1983: The ventilated thermocline. *J. Phys. Oceanogr.,* **13,** 292–309.

Macdonald, A. M., 1993: Property fluxes at 30°S and their implications for the Pacific–Indian throughflow and the global heat budget. *J. Geophys. Res.,* **98,** 6851–6868.

——, 1998: The global ocean circulation: A hydrographic estimate and regional analysis. *Progress in Oceanography,* Vol. 41, Pergamon, 281–382.

McCartney, M. S., 1982: The subtropical recirculation of mode waters. *J. Mar. Res.,* **40** (Suppl.), 427–474.

Orsi, A. H., G. C. Johnson, and J. L. Bullister, 1999: Circulation, mixing, and production of Antarctic Bottom Water. *Progress in Oceanography,* Vol. 43, Pergamon, 55–109.

Parrilla, G., A. Lavin, H. Bryden, M. Garcia, and R. Millard, 1994: Rising temperatures in the subtropical North Atlantic Ocean over the past 35 years. *Nature*, **369,** 48–51.

Reid, J. L., 1994: On the total geostrophic circulation of the North Atlantic Ocean: Flow patterns, tracers and transports. *Progress in Oceanography,* Vol. 33, Pergamon, 1–92.

——, 1997: On the total geostrophic circulation of the Pacific Ocean: Flow patterns, tracers and transports. *Progress in Oceanography,* Vol. 39, Pergamon, 263–352.

——, 2002: On the total geostrophic circulation of the Indian Ocean: Flow patterns, tracers and transports. *Progress in Oceanography,* in press.

Rintoul, S., 1991: South Atlantic interbasin exchange. *J. Geophys. Res.,* **96,** 2675–2692.

Roach, A. T., K. Aagaard, C. H. Pease, S. A. Salo, T. Weingartner, V. Pavlov, and M. Kulakov, 1995: Direct measurements of transport and water properties through the Bering Strait. *J. Geophys. Res.,* **100,** 18 443–18 457.

Robbins, P. E., and J. M. Toole, 1997: The dissolved silica budget as a constraint on the meridional overturning circulation of the Indian Ocean. *Deep-Sea Res.,* **44,** 879–906.

Roemmich, D., 1980: Estimation of meridional heat flux in the North Atlantic by inverse methods. *J. Phys. Oceanogr.,* **10,** 1972–1983.

——, and C. Wunsch, 1985: Two transatlantic sections: Meridional circulation and heat flux in the subtropical North Atlantic Ocean. *Deep-Sea Res.,* **32,** 619–664.

——, and T. McCallister, 1989: Large scale circulation of the North Pacific Ocean. *Progress in Oceanography,* Vol. 22, Pergamon, 171–204.

——, J. Gilson, B. Cornuelle, and R. Weller, 2001: Mean time-varying meridional transport of heat at the tropical subtropical boundary of the North Pacific Ocean. *J. Geophys. Res.,* **106,** 8957–8970.

Sato, O. T., and T. Rossby, 2000: Seasonal and low-frequency variability of the meridional heat flux at 36°N in the North Atlantic. *J. Phys. Oceanogr.,* **30,** 606–621.

Schmitz, W. J., 1995: On the interbasin-scale thermohaline circulation. *Rev. Geophys.,* **33,** 151–173.

Sloyan, B. M., and S. R. Rintoul, 2001a: The Southern Ocean limb of the global deep overturning circulation. *J. Phys. Oceanogr.,* **31,** 143–173.

——, and ——, 2001b: Circulation, renewal, and modification of Antarctic mode and intermediate water. *J. Phys. Oceanogr.,* **31,** 1005–1030.

Talley, L. D., 1984: Meridional heat transport in the Pacific Ocean. *J. Phys. Oceanogr.,* **14,** 231–241.

——, 1996: Antarctic Intermediate Water in the South Atlantic. *The South Atlantic: Present and Past Circulation,* G. Wefer et al., Eds., Springer-Verlag, 219–238.

——, 1999: Some aspects of ocean heat transport by the shallow, intermediate and deep overturning circulations. *Mechanisms of Global Climate Change at Millennial Time Scales, Geophys. Monogr.,* Vol. 112, Amer. Geophys. Union, 1–22.

Toole, J. M., and B. A. Warren, 1993: A hydrographic section across the subtropical South Indian Ocean. *Deep-Sea Res.,* **40,** 1973–2019.

Trenberth, K. E., and J. M. Caron, 2001: Estimates of meridional atmosphere and ocean heat transports. *J. Climate,* **14,** 3433–3443.

——, J. M. Caron, and D. P. Stepaniak, 2001: The atmospheric energy budget and implications for surface fluxes and ocean heat transports. *Climate Dyn.,* **17,** 259–276.

Tsimplis, M. N., H. L. Bryden, and S. Bacon, 1998: The circulation of the subtropical South Pacific derived from hydrographic data. *J. Geophys. Res.,* **103,** 21 443–21 468.

Vranes, K., A. L. Gordon, and A. Ffield, 2002: The heat transport of the Indonesian Throughflow and implications for the Indian Ocean heat budget. *Deep-Sea Res.,* **49B,** 1391–1410.

Wijffels, S. E., 2001: Ocean transport of fresh water. *Ocean Circulation and Climate,* G. Siedler, J. Church, and J. Gould, Eds., Academic Press, 475–488.

——, R. W. Schmitt, H. L. Bryden, and A. Stigebrandt, 1992: Transport of freshwater by the oceans. *J. Phys. Oceanogr.,* **22,** 155–162.

——, J. M. Toole, H. L. Bryden, R. A. Fine, W. J. Jenkins, and J. L. Bullister, 1996: The water masses and circulation at 10°N in the Pacific. *Deep-Sea Res.,* **43,** 501–544.

——, ——, and R. Davis, 2001: Revisiting the South Pacific subtropical circulation: A synthesis of World Ocean Circulation Experiment observations along 32°S. *J. Geophys. Res.,* **106,** 19 481–19 514.

Wunsch, C., D. Hu, and B. Grant, 1983: Mass, heat, salt and nutrient fluxes in the South Pacific Ocean. *J. Phys. Oceanogr.,* **13,** 725–753.

Yuan, X., and L. D. Talley, 1992: Shallow salinity minima in the North Pacific. *J. Phys. Oceanogr.,* **22,** 1302–1316.